LOW-COST LED LUMINAIRE FOR GENERAL ILLUMINATION

Final Report

Period Start Date:	**August 1, 2012**
Period End Date:	**July 31, 2014**
Principal Investigator:	**Ted Lowes**
Date Report Issued:	**November 4, 2014**
Award Number:	**DE-EE0005846**
Project Manager:	**Joel Chaddock**

CREE Santa Barbara Technology Center

340 Storke Road

Goleta CA 93117

(805) 968-9460

EXECUTIVE SUMMARY

During this two-year Solid-State Lighting (SSL) Manufacturing R&D project Cree developed novel light emitting diode (LED) technologies contributing to a cost-optimized, efficient LED troffer luminaire platform emitting at ~3500K correlated color temperature (CCT) at a color rendering index (CRI) of >90. To successfully achieve program goals, Cree used a comprehensive approach to address cost reduction of the various optical, thermal and electrical subsystems in the luminaire without impacting performance. These developments built on Cree's high- brightness, low-cost LED platforms to design a novel LED component architecture that will enable low-cost troffer luminaire designs with high total system efficacy. The project scope included cost reductions to nearly all major troffer subsystems as well as assembly costs. For example, no thermal management components were included in the troffer, owing to the optimized distribution of compact low- to mid-power LEDs. It is estimated that a significant manufacturing cost savings will result relative to Cree's conventional troffers at the start of the project.

A chief project accomplishment was the successful development of a new compact, high-efficacy LED component geometry with a broad far-field intensity distribution and even color point vs. emission angle. After further optimization and testing for production, the Cree XQ series of LEDs resulted. XQ LEDs are currently utilized in Cree's AR series troffers, and they are being considered for use in other platforms. The XQ lens geometry influenced the independent development of Cree's XB-E and XB-G high-voltage LEDs, which also have a broad intensity distribution at high efficacy, and are finding wide implementation in Cree's omnidirectional A-lamps.

DISCLAIMER

TABLE OF CONTENTS

PROJECT OBJECTIVES

The focus of this manufacturing program was the development of a low-cost, high-efficacy light emitting diode (LED) architectural troffer suitable for indoor illumination. This 2' x 4' troffer was to provide 4,000 lumens and 90 lumens per watt (LPW) at 3500K correlated color temperature (CCT) and a color rendering index (CRI) of 90, matching today's state-of-the-art performance. This product would also provide a minimum lifetime of 50,000 hours with a color shift of less than 2-step MacAdam ellipse. The cost was to be reduced 30% to an end-user price of $160 or less. To achieve the program goals, Cree used a comprehensive approach to address the cost reduction of the various optical, thermal and electrical subsystems in the luminaire without impacting performance. The scope of work included developing a primary beam-shaping LED optic that enabled a lower-cost structure in the resulting luminaire design.

PROBLEM BACKGROUND

Solid-state lighting based on LEDs has emerged as a superior alternative to inefficient conventional lighting, particularly incandescent. LED lighting can lead to 80 percent energy savings; can last 50,000 hours – 2-50 times longer than most bulbs; and contains no toxic lead or mercury. However, to enable mass adoption, particularly at the consumer level, the cost of LED luminaires must be reduced by an order of magnitude while achieving superior efficiency, light quality and lifetime.

To become viable, energy-efficient replacement solutions must deliver system efficacies of > 90 LPW with excellent color rendering (CRI > 90, or comparable) at a cost that enables payback periods of two years or less for commercial applications. This development will enable significant site energy savings as it targets commercial and retail lighting applications that are most sensitive to the lifetime operating costs with their extended operating hours per day. If costs are reduced substantially, dramatic energy savings can be realized by replacing incandescent lighting in the residential market as well.

In light of these challenges, Cree proposed to develop a cost-effective LED troffer platform enabling significant cost reductions relative to existing form factors without sacrificing performance. A key development was the development of low-cost, compact LEDs with broad far-field emission distribution, which enabled the use of an efficient direct-view diffusion scheme.

TECHNICAL APPROACH

This SSL manufacturing development project built on Cree's SC3 LED platform to design a 2'x4' architectural troffer with 30% lower cost than Cree's CR24 troffer at the start of the project, without compromising performance or reliability. To meet the program goals, Cree used a holistic approach to system design in order to optimize optical, thermal and mechanical integration trade-offs. The scope of work included improvements to the LED luminous intensity distribution, optimized color mixing, thermal management and optic integration into a simplified housing. The reliability of the new light engine was assessed under accelerated testing conditions. During the program, Cree demonstrated production-capable, efficient, and reliable solid state lighting manufacturing methods at significant cost reductions compared to current products.

The primary tasks are summarized as follows:

Task 1. Program Management: The interdependent tasks listed below will be managed and monitored by utilizing the Project Management Plan outlined in detail in this communication. Cross-functional team contributions must be coordinated and integrated to maximize value of new designs, processes and technologies that become available throughout the contract work. The technical progress will be continuously monitored against the program milestones using this Project Management Plan.

Task 2. Light Engine Development: Under this task, Cree will develop a new light engine platform based on a custom LED primary optic to provide a lower cost structure for the troffer light engine. The LED primary optic is intended to have a broader emission pattern than conventional hemispherical domed packages, while also exhibiting sufficient color mixing to enable a direct-view troffer configuration that does not require excessive secondary diffusion optics. The light engine will be a comprehensive integration of different technology elements involving optical design, mechanical design and thermal management. The light engine will offer cost reduction benefits without impacting overall system efficiency or reliability.

Task 3. Fixture Design and Development: Cree will design a troffer fixture with integrated cost-effective thermal management and diffusing optics. A direct-view approach is the primary approach for lowering manufacturing costs by simplifying design and reducing the number and size of components. This will be enabled by leveraging the innovations developed in the troffer light engine carried out in Task 2. The target optical efficiency of the assembled troffer is > 90%.

Task 4. Luminaire Integration: Cree will integrate the light engine and fixture subsystems developed in Tasks 2 and 3 into the final 2’ x 4’ assembled troffer with equivalent performance to Cree’s CR24 troffer, but at significantly reduced cost. The light engine and fixture assembly will be combined with a state-of-the art electrical driver with dimming capability to produce the final luminaire demonstrator. Performance will be characterized by measurements that follow the LM 79 protocol for LED luminaire testing.

Work Schedule

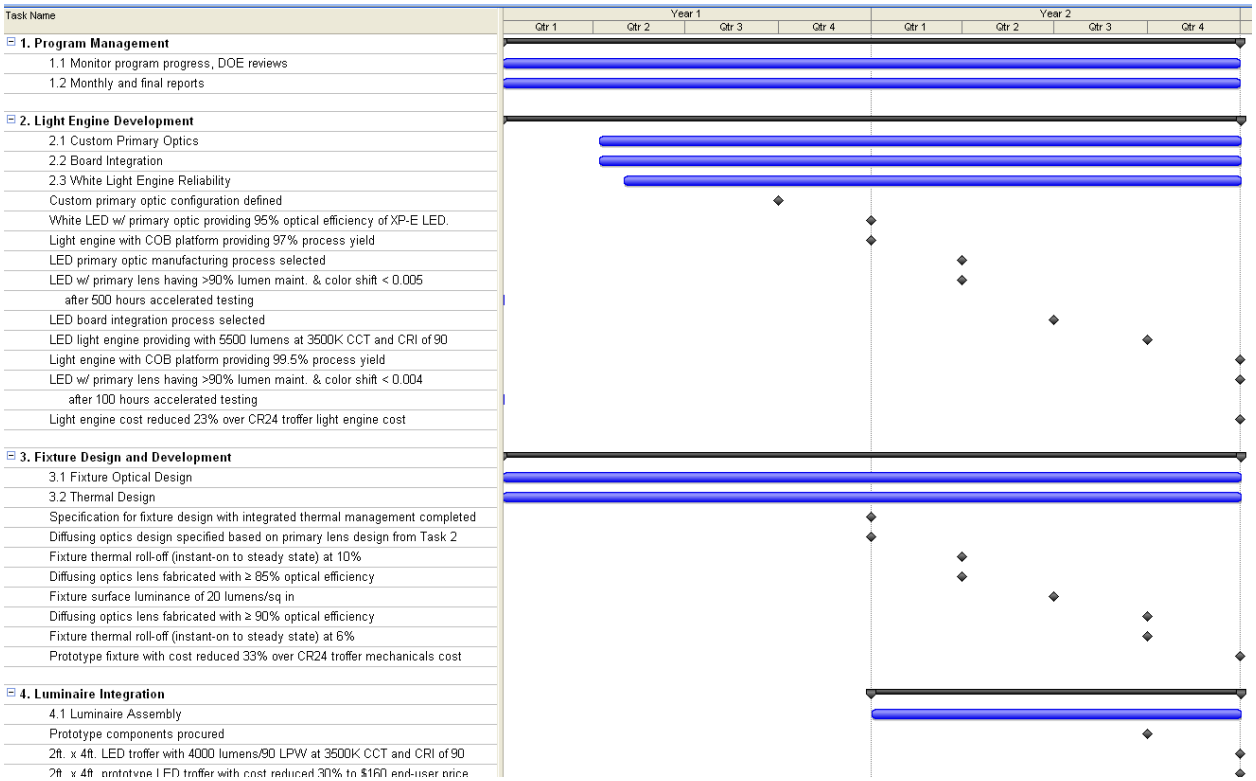

TECHNICAL ACCOMPLISHMENTS

Task 2 – Light Engine Development

Task 2.1 – Custom Primary Optic Definition

Package Optics Design

A central goal of the project was the development of a compact, high-efficacy LED package with broad far-field emission favorable for direct-view troffer geometries. Given a chosen LED package footprint, an important package parameter is lens geometry, particularly for our prototype package geometry in which optical modeling predicted a higher degree of light "recycling" than conventional domed packages. We therefore studied variations in luminous flux and color point as a function of lens aspect ratio (height to width), while also monitoring package efficacy to determine if there were tradeoffs among these characteristics. Lens aspect ratio was varied within a range anticipated to be practical for commercial production, for three color temperature ranges (~3000K, ~4000K, ~5500K) to determine if the influence of lens aspect ratio on LED emission changed based on differing amounts of phosphor applied to the chip. Testing was conducted using a goniometer for far-field emission variation vs. angle, and an integrating sphere for efficacy and color point. The color point groupings of each sample set are shown in Fig. 1, which shows LEDs falling tightly into ~2 color bins (~4 MacAdam ellipse steps) for each set. Fig. 1 also shows changes in color temperature as a function of lens aspect ratio for each data

set. CCT varied by as much as 250K when lens aspect ratio increased in the 4000K and 5500K data sets, but was nearly constant for the ~3000K sample set.

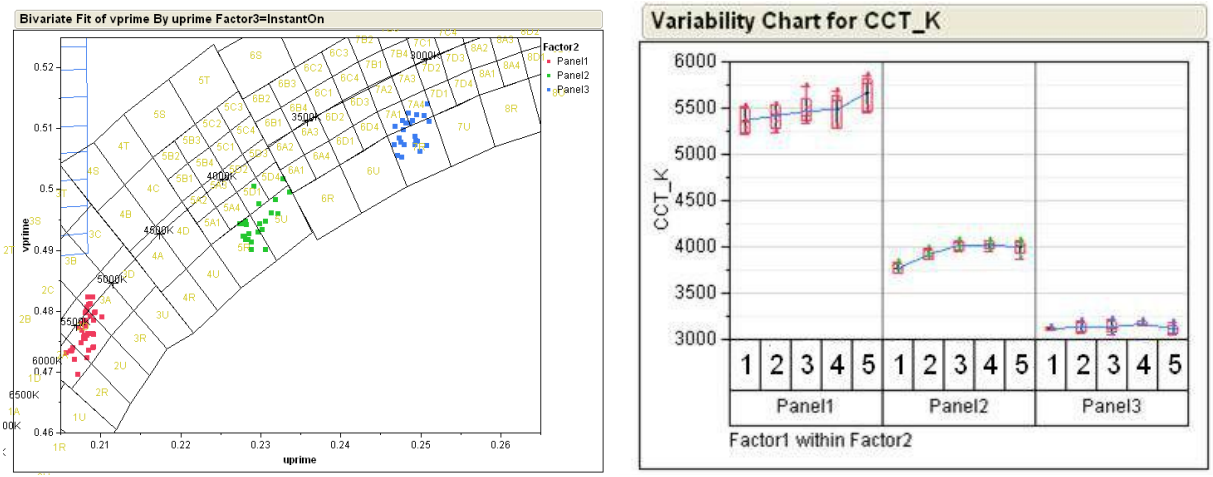

Fig. 1. left: Color point measurements of data sets grouped about 3000K, 4000K, and 5500K color temperatures. right: color temperature variation vs. lens aspect ratio for each data set.

The variation in color point coordinates (u',v') vs. lens aspect ratio was also quantified, as shown in Fig. 2. Coordinate values shifted by up to ~0.006 as lens aspect ratio was varied, with the v' coordinate typically showing more variation at a given color temperature than u'.

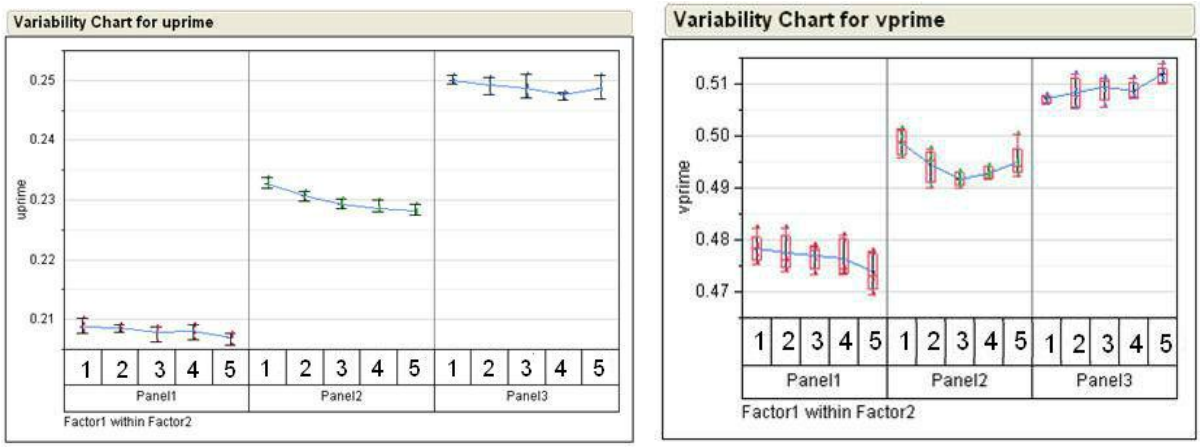

Fig. 2. left: Variation in color coordinate u' vs. lens aspect ratio (1-5) at color temperatures of ~5500K (panel 1), 4000K (panel 2), and 3000K (panel 3). right: Variation in color coordinate v' vs. lens aspect ratio.

Prototype LED package emission characteristics vs. viewing angle from normal are shown in Fig. 3. While luminous flux variation profiles vs. angle were fairly consistent at each lens aspect ratio value, the flux profiles at selected angles varied significantly among different lens aspect ratios. More than one lens aspect ratio was expected to have emission profiles advantageous for our proposed direct-view troffer design. This study illustrated the need to consider lens aspect ratio as a key LED package geometry parameter, since the emission profile was anticipated to directly influence our choice of secondary optics (diffuser) in the troffer.

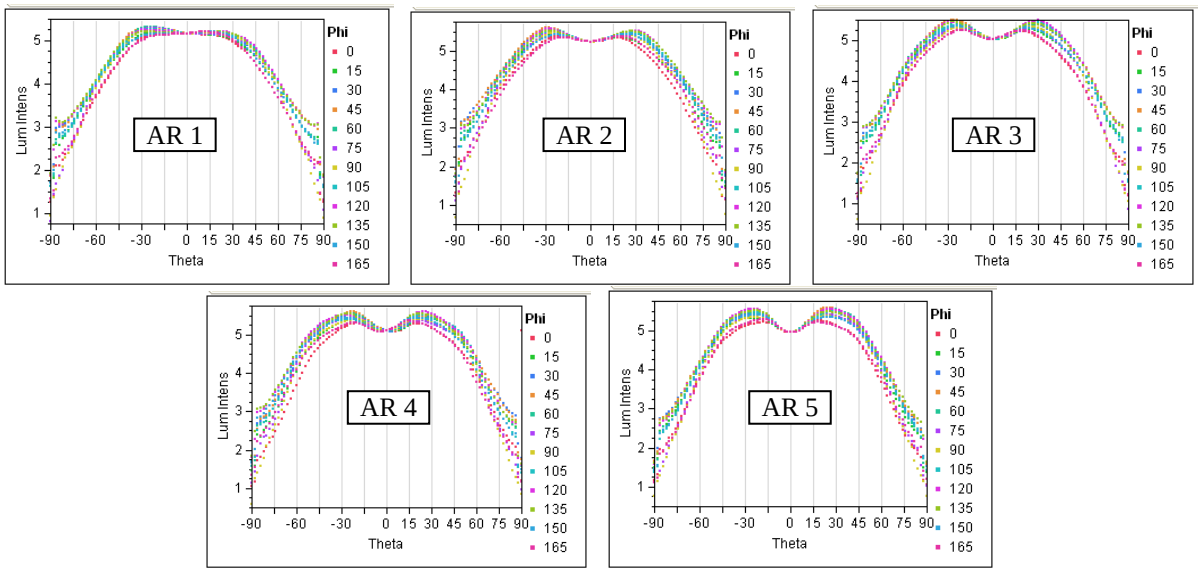

Fig. 3. Variation in prototype package luminous flux vs. viewing angle from normal for differing lens aspect ratio (AR) values. The package emission variation vs. angle changes significantly over the aspect ratio range studied.

Finally, we considered the effect of package lens aspect ratio on LED efficacy (in lm/W) in each color temperature range (see Fig. 4). For all color temperatures studied, efficacy increased by 5-6% over the lens aspect ratio ranged studied. Thus given a satisfactory LED luminous flux and color point variation vs. emission angle, we favored larger lens aspect ratio values for LEDs installed in our proposed direct-view troffer configuration.

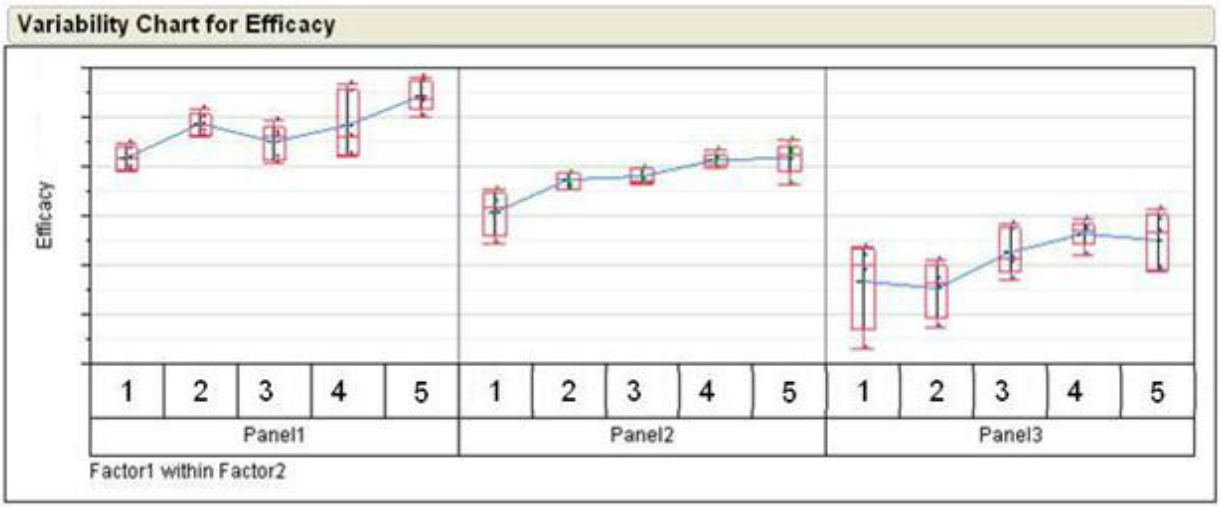

Fig. 4. LED package efficacy (relative units) vs. lens aspect ratio for three different color temperature ranges (~5500K, ~4000K, ~3000K).

Substrate Reflective Coatings

We observed that light absorption by the prototype package substrate and materials deposited upon it (*e.g.* metal traces) were a likely source of optical loss in the prototype package. In the effort to improve prototype LED package efficacy, we developed a highly reflective coating that could be applied to the substrate surface while not interfering with light emission from the chips,

even at high emission angles from normal. In addition, this coating was required to be chemically and mechanically compatible with the rest of the LED, and thus not adversely affect LED reliability when exposed to elevated temperature or luminous flux.

We evaluated several candidate reflective material formulations (A, C, S) that could be applied via cost-effective, scalable methods in production. Each material type was applied in varying thicknesses to establish the dependence of peak reflectivity, with the goal of obtaining high reflectivity at low thickness (thereby minimizing the effect that the reflective layer has on the overall LED geometry). As shown in Fig. 5, a wide range of reflectivity values was observed, with formulations C-2 and C-3 among the best, followed closely by formulation A-1. We confirmed that these formulations had a relatively constant reflectivity over the wavelength range of interest, as shown in Fig. 6. Therefore we did not expect the reflective coatings to have a significant effect on color mixing by absorbing one color more than another, for example.

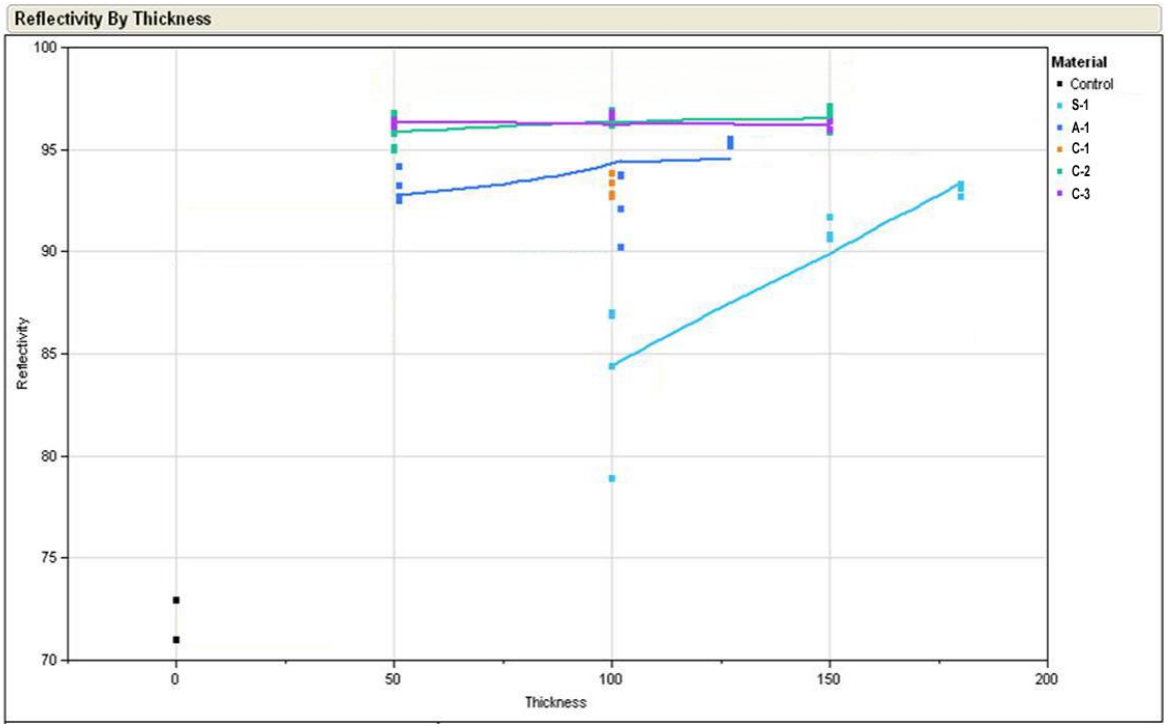

Fig. 5. Reflectivity vs. thickness for several formulations of reflective coating to be incorporated into the prototype LED package. The control sample was an uncoated metal coupon. The in-house formulations C-2 and C-3 exhibited the highest reflectivity, followed closely formulation A-1.

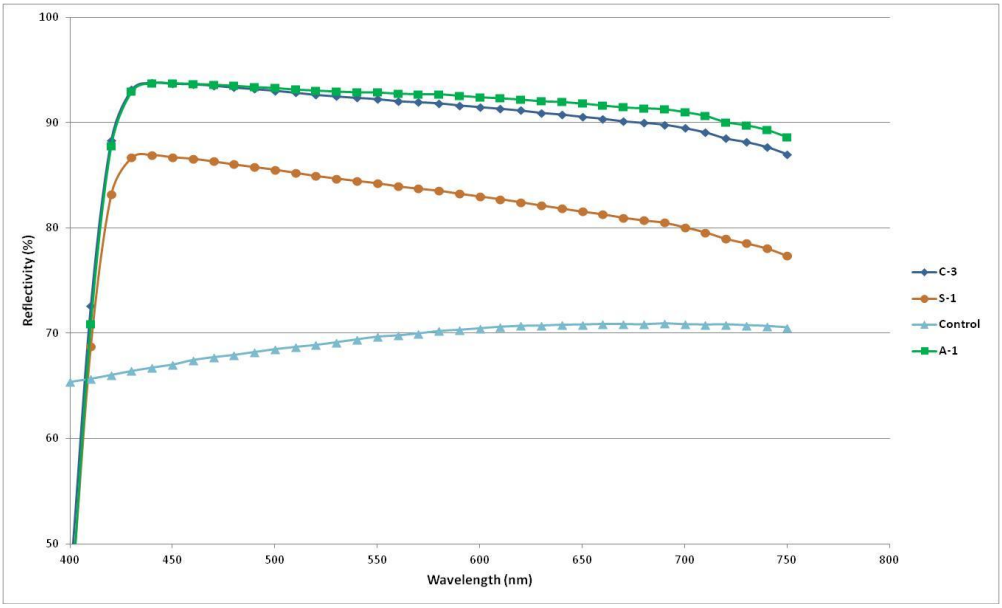

Fig. 6. Reflectivity vs. wavelength for coating formulations, as coated on a control metal surface.

In addition to measuring as-deposited coating reflectivity, we also put the coatings through a simulated heating/cooling temperature cycle that they would experience during an LED solder re-flow process. We found that although the reflectivity of all coatings dropped slightly after exposure to this cycle (Fig. 7), the reflectivity values of the C-3 and A-1 coatings remained high enough to justify their continued study in fabricated LEDs. We proceeded to incorporate the coatings into fully built LED packages to establish their benefit on efficacy compared to packages with un-coated substrates.

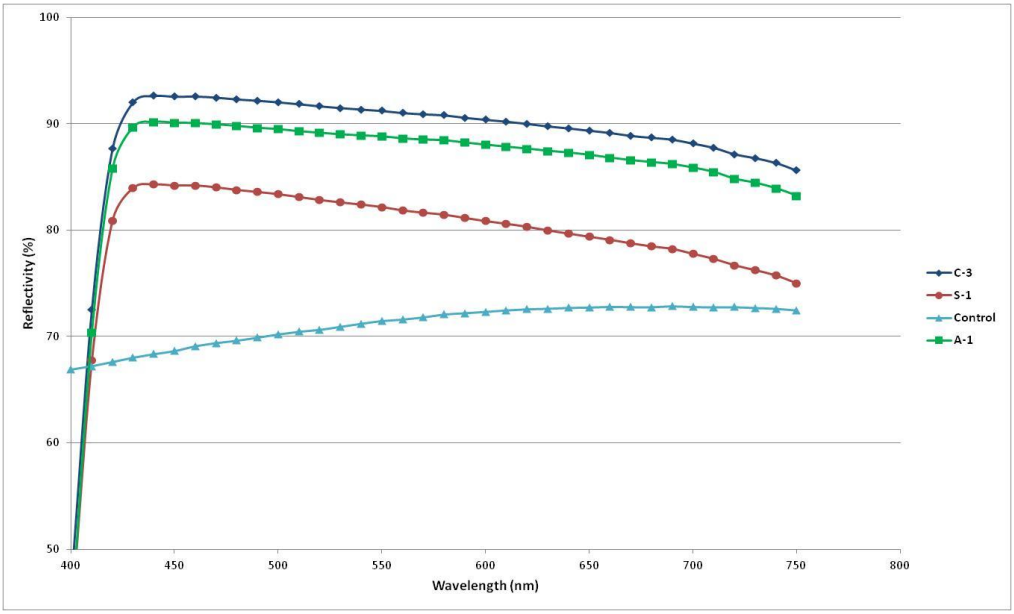

Fig. 7. Reflectivity vs. wavelength for coating formulations after temperature cycling through a simulated solder reflow process.

Reflective coatings were applied to trace-patterned LED substrate panels using processes in which all LED positions on the panel were simultaneously selectively coated prior to chip attach. The area fraction of the coating (and therefore its proximity to the chips) was varied widely over seven panel sections (1-7, in decreasing order of coverage) to determine its effect on LED luminous flux and chip attach yield; micrographs of selected area fractions are shown in Fig. 8.

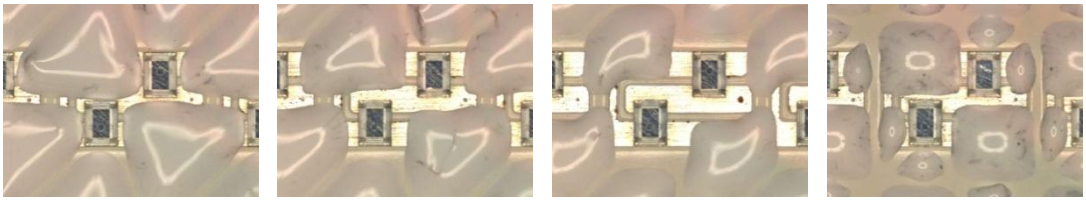

Fig. 8. Micrographs of solder-attached chips after reflective coating application in panel sections 1, 3, 5, and 7, with decreasing area fraction of coverage from left to right.

After chip attach, all LED component positions on substrate panels were probed for light emission (and therefore electrical continuity), an example of which is plotted in Fig. 9. An overall electrical yield of 99% resulted, with failures only on the top and bottom rows, which were traced to panel handling and securing methods during reflective coating application. This was a positive indication that despite narrow spacings between the coating and the chips, our standard chip solder attach procedure did not need to be altered to accommodate the coating.

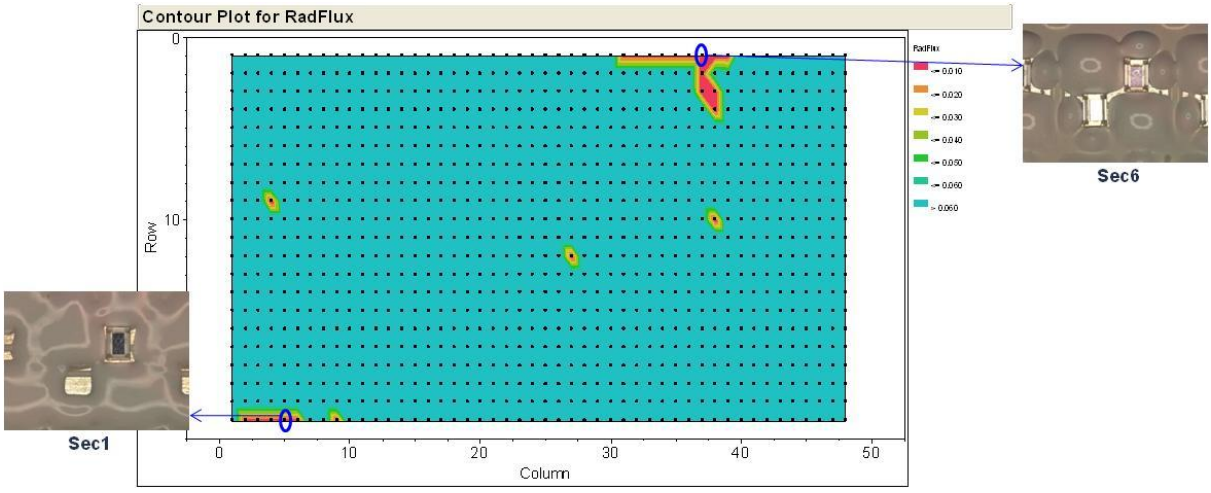

Fig. 9. Plot of LED blue chip radiant flux vs. panel position, with failures highlighted at lower left and upper right. Note that the three failures in the middle were panel flaws previously identified and marked by the vendor, and therefore not counted.

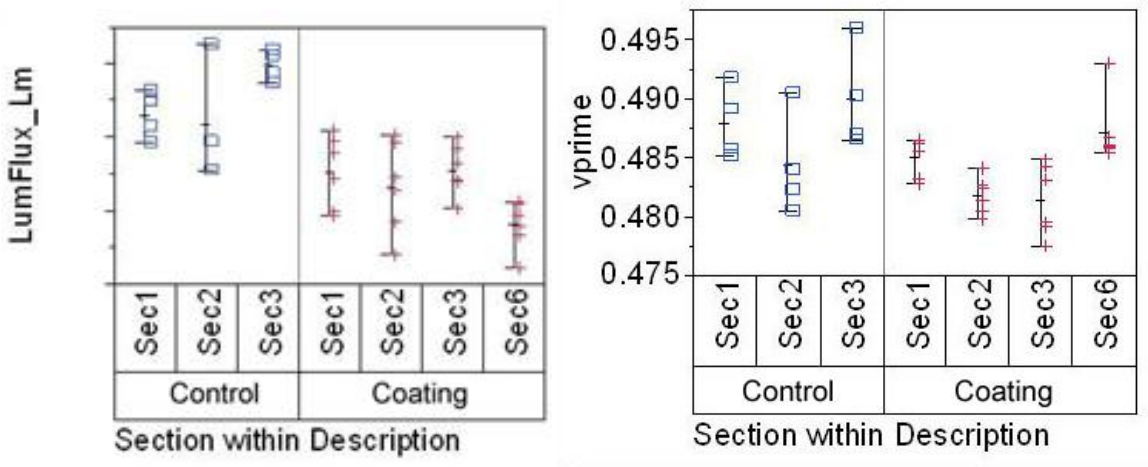

Fig. 10. Luminous flux (relative units) and v' color coordinate of prototype LEDs with ("Coating") and without ("Control") reflective coating surrounding the chips.

Prototype LEDs containing a reflective substrate coating were fabricated and tested for comparison with identical LEDs lacking the coating. As shown in Fig. 10, we obtained the unexpected result that the average luminous flux of LEDs with the coating was actually *lower* than those without it, recorded at similar color points. This counterintuitive result was traced to the profile of the coating itself: it was found to be too thick compared to the chips. The resultant blocking of side-emitted light from the chips manifested as lower overall LED luminous flux.

We then pursued modifications to both the reflective coating characteristics and application techniques to better control coating profile at lower thicknesses. Through several iterations of process improvement, we determined that the reflective coating could be applied at lower thickness with minimized variation in thickness as well as shape in selectively applied layers. When these improved methods were applied to fully fabricated prototype LEDs, a significant improvement in total luminous flux resulted, as shown in Fig. 11. At the low end of the coating thickness range studied, the luminous flux gain was the highest.

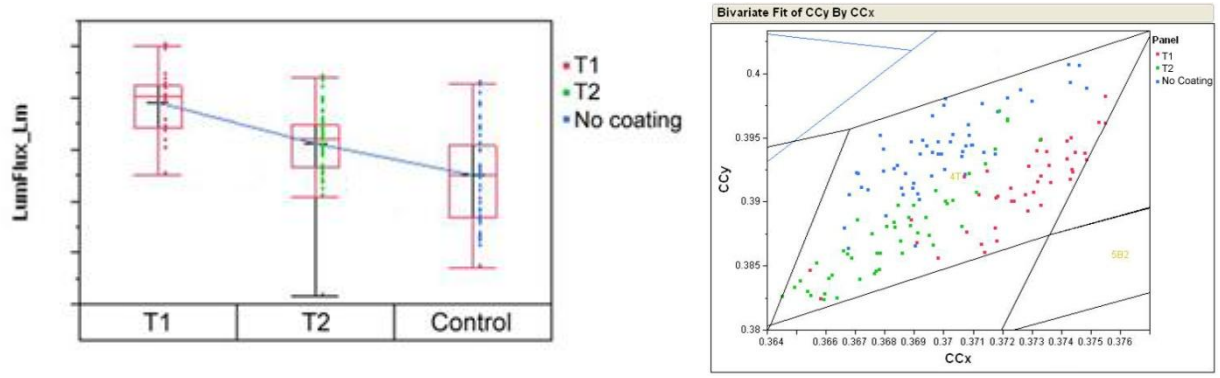

Fig. 11. Luminous flux (left) and color coordinates (right) for prototype LEDs with thin reflective substrate coatings relative to control LEDs with no coating.

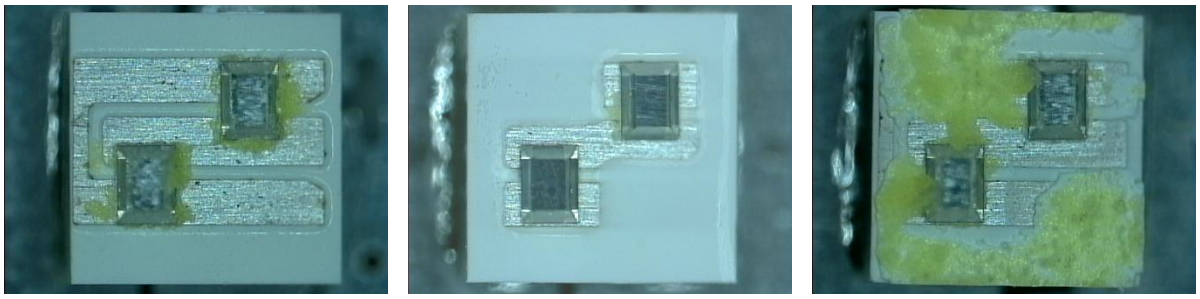

Fig. 12. Micrographs of prototype LED package substrates after lens shear: uncoated substrate (left); substrate covered by reflective coating (center); substrate covered by reflective coating treated prior to phosphor layer application (right). The failure mode of the center micrograph was loss of adhesion at the interface between the reflective coating and the phosphor-containing layer.

As part of our reflective substrate coating evaluation, we quantified the degree of LED lens adhesion to the coated package substrate via lens shear measurements. In this method, a carefully positioned blade is pushed against the side of the lens until it separates from the package substrate. This test is a useful indication of how well the LEDs will survive post-fabrication handling. For the baseline prototype LED lens aspect ratio, we found that the lens shear strength was significantly lower when the reflective coating was implemented. This suggested that the interface between the coating and the phosphor-containing layer was of low adhesive strength, which was confirmed via numerous measurements and visual inspections of the post-shear substrate surfaces, as shown in Fig. 12. For an uncoated substrate ("control" case), the shear occurred within the phosphor-containing layer and via delamination from the package substrate surface. When a reflective coating was used, the failure mode was loss of adhesion at the interface between this coating and the phosphor-containing layer. The failure mode changed to cohesive shear within the phosphor layer when the reflective coating was treated prior to phosphor layer application (see below).

In response to the lowered lens shear values obtained when the reflective coating was implemented, we investigated the effects of various treatments to the coating surface prior to phosphor layer application. After several iterations of fabrication and testing, we selected a readily scalable and cost-effective surface treatment. As shown in Fig. 13, this treatment was effective at restoring the lens shear values of packages with coated substrates to levels on par or higher than those with no coating, regardless of coating setback (separation distance from dies).

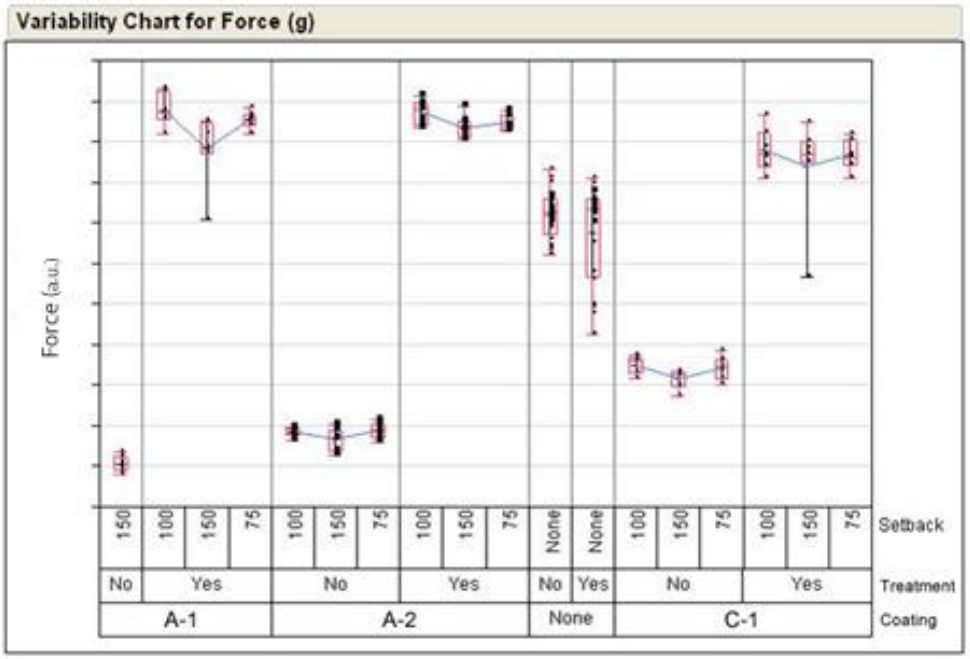

Fig. 13. Lens shear strength for three reflective coating formulations with various coating-die setback (separation) values, and with or without coating treatment prior to phosphor layer application.

To quantify the die attach yields in large populations of prototype packages with reflective substrate coatings, we developed a hybrid testing method consisting of a combination of forward voltage (V_f) and thermal resistance (R_{th}) measurements. We found that this method was necessary for multi-chip packages in which the chips are connected in parallel; a conventional measurement of V_f alone was insufficient to screen for chip attach failures. Based on conservative engineering judgment, failure criteria were set at: V_f > 100mV above the panel mean V_f, and R_{th} > 4°C/W from the panel mean R_{th} (typically ~16 °C/W). An example of this analysis is shown in Fig. 14, in which it can be readily determined which packages fail based on V_f, R_{th}, or both. Co-plotting both characteristics enables screening of packages with one or more failed die attach locations, which can then be inspected to determine the failure mechanism. We anticipate the pass/failure criteria will be refined in the manufacturing environment where sample sizes for statistical analysis increase, coupled with root cause analysis for the failed units.

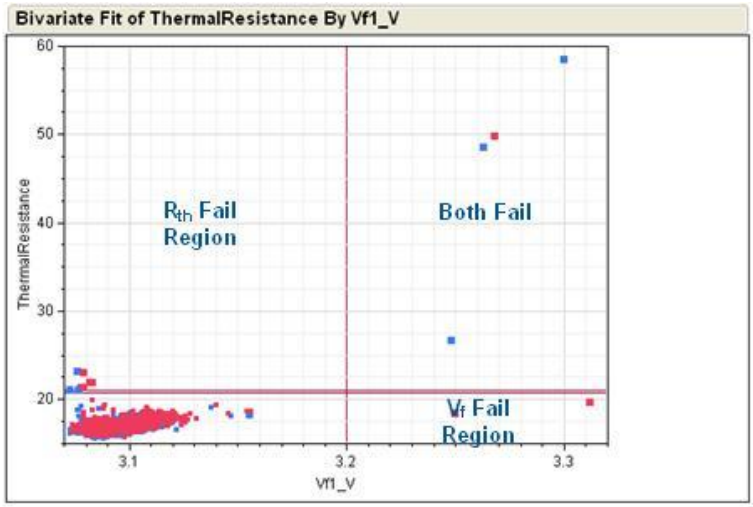

Fig. 14. A plot combining V_f and R_{th} values for two prototype LED panels, which illustrates the utility of using both characteristics as pass/fail criteria in determining die attach yield when a reflective substrate coating is used.

Prototype LEDs containing a reflective substrate coating were fabricated and tested for comparison with identical LEDs lacking the coating. We measured the luminous flux and color temperature variation as a function of emission angle (see Fig. 15), and established that there were few differences in these characteristics between prototype packages with the reflective coating vs. those lacking it. This indicated that no modifications were needed to the lens primary optic (lens) geometry when utilizing the reflective substrate coating.

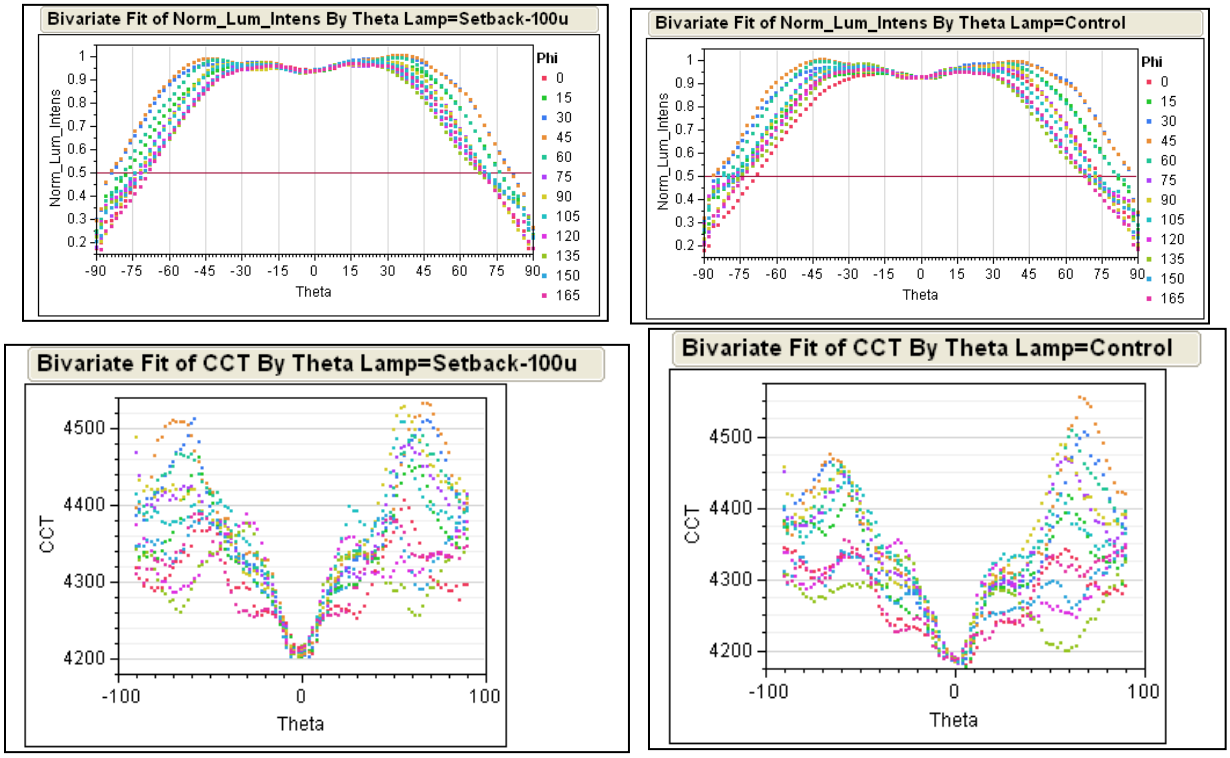

Fig. 15. Plots of luminous flux (top row) and color temperature (bottom row) vs. emission angle for prototype LED packages with (left) and without (right) a reflective coating applied to the package substrate surface. There are very minor differences in flux and CCT for the two cases.

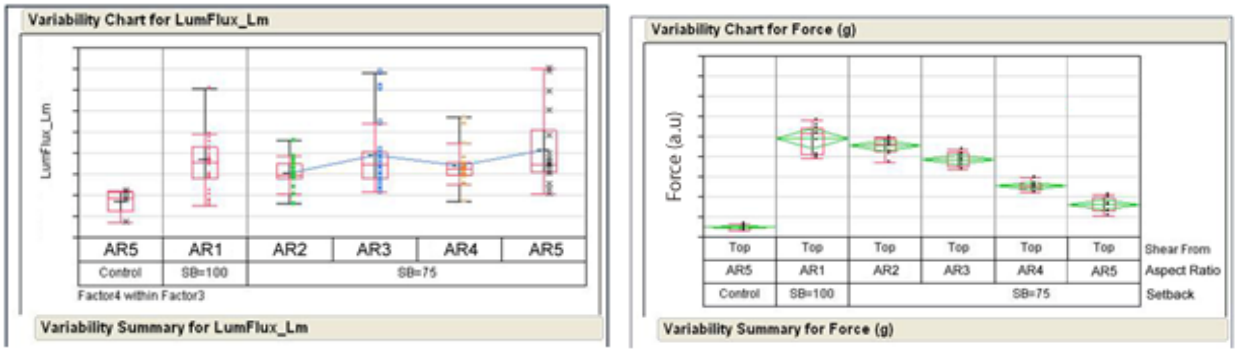

Fig. 16. Left: relative luminous flux from prototype packages of various lens aspect ratios (ARx) with a reflective substrate coating, compared to a package with no coating and a high aspect ratio (Control). Right: lens shear strength of the aspect ratios relative to a control with no reflective coating and of the highest aspect ratio.

We performed LF measurements on prototype packages containing the reflective substrate coating. As evident in Fig. 16, the LF at low lens aspect ratio was maintained compared to higher aspect ratios when the reflective substrate coating is implemented. In addition, the luminous flux for all package aspect ratios with reflective coating was higher than the control case. This finding could benefit the manufacturing cost of the prototype package, since less silicone is needed in the lens primary optic. In addition, prototype packages with lower aspect ratio had higher lens shear strength values, as shown in Fig. 16. This is an attractive feature for the robustness of the LEDs while being handled during fabrication and placement into luminaires.

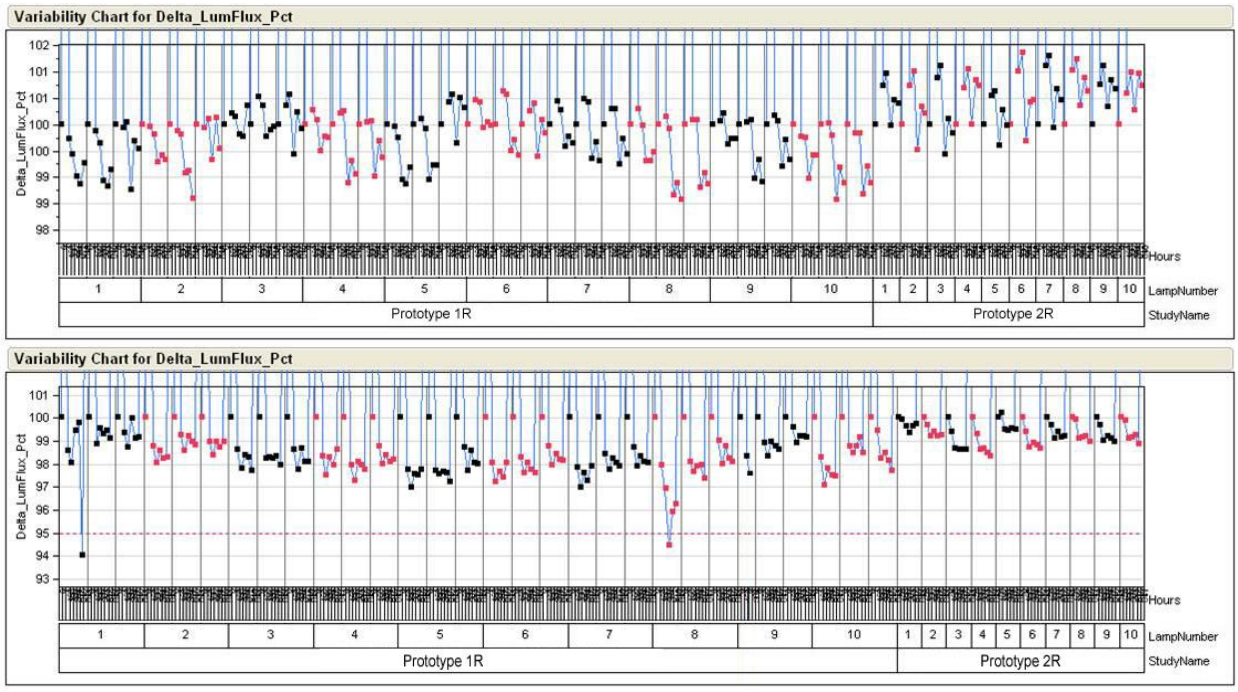

Fig. 17. Luminous flux during high-temperature (top) and high-temperature/high-humidity (bottom) accelerated testing of prototype packages in two configurations at 840 hrs.

The luminous flux and color point maintenance of prototype packages with reflective substrate coating were tested under Cree's standard accelerated aging conditions to ensure that

the coating would not adversely affect long-duration package performance, *e.g.* via chemical reaction. As shown in Fig. 17, at 840 hrs. prototype LEDs tested at high temperature as well as a combination of high temperature and high humidity exhibited little luminous flux change, with only a few packages falling below 95% of starting luminous flux; the vast majority remained above 97%.

Likewise, the color point shift of prototype LEDs with a reflective substrate coating was minor (Fig. 18), with changes of 0.002-0.003 in u' and v' within 840 hrs. of testing in high-temperature/high-humidity conditions. This, in combination with the luminous flux maintenance data above, indicated the robustness of the prototype LED package under demanding operating conditions.

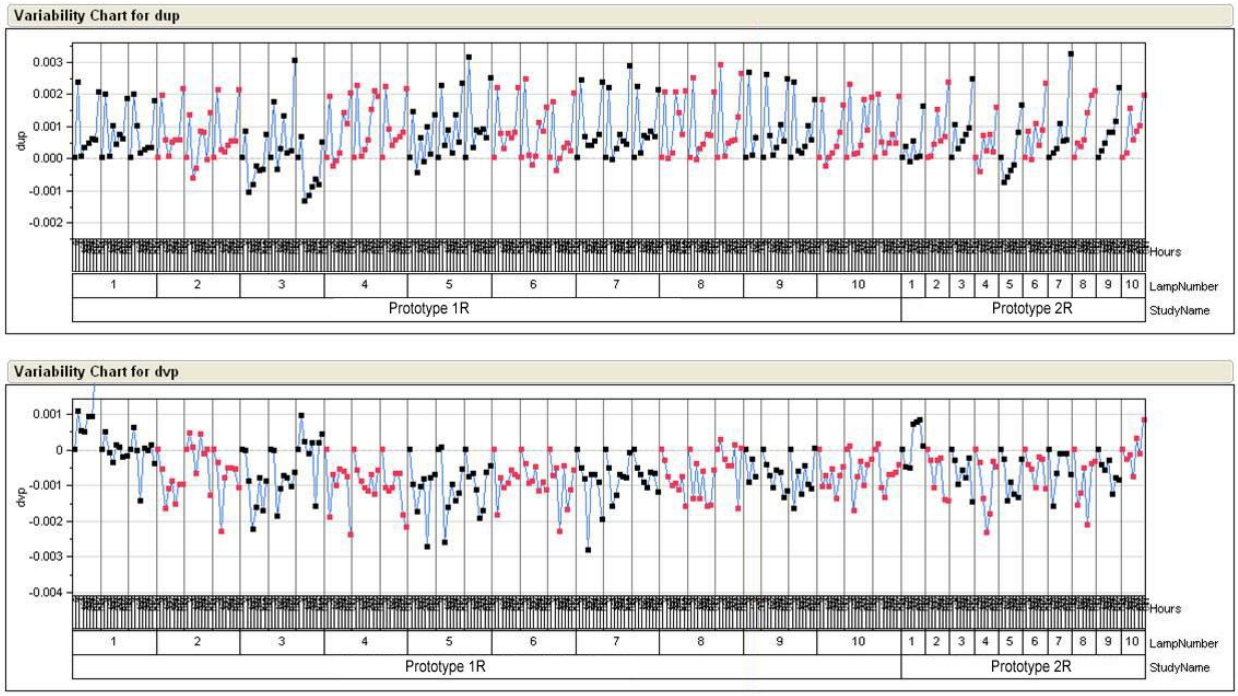

Fig. 18. Color point variation (top: u', bottom: v') of prototype LEDs (two configurations) with reflective substrate coating during high-temperature/high-humidity accelerated testing, at 840 hrs. Changes of 0.002-0.003 in u' and v' color point coordinates were observed.

In an effort to confirm the reproducibility of the reflective coating application process and therefore its feasibility for full-scale production, we fabricated several lots of prototype LEDs. We quantified die attach yield using the combined thermal resistance / forward voltage method described above, with the result that for over 8,000 coating packages tested, 99.3% passed our yield criteria, which is comparable to the value for packages with no reflective coating.

Table 1. Numbers of prototype packages vs. control packages passing yield criteria.

Build#	Reflective Coating	Control
B9-P1	251/252	252/252
B9-P5	252/252	252/252
B10-P1	831/840	168/168
B10-P3	834/840	167/168
B10-P5	828/840	165/168
B12-P1	833/833	162/163
B12-P2	816/826	164/165
B12-P3	817/820	168/168
B12-P4	826/830	167/167
B12-P5	827/832	165/165
B12-P6	835/838	167/167
Total / Avg	7950/8003	1997/2003
Ave. % Yield	**99.3%**	**99.7%**

For several lots of this series of LED builds, we also confirmed the reproducibility of the luminous flux gain enabled by the reflective substrate coating. Packages with and without the coating were measured individually in an integrating sphere to quantify their luminous flux, which was time consuming but less susceptible to variation than our previously conducted on-panel testing in which packages were measured while still surrounded by their nearest neighbors on the substrate panel (*i.e.* prior to singulation). As shown in Fig. 19, LF gains were consistently observed for packages utilizing the reflective coating vs. those lacking it.

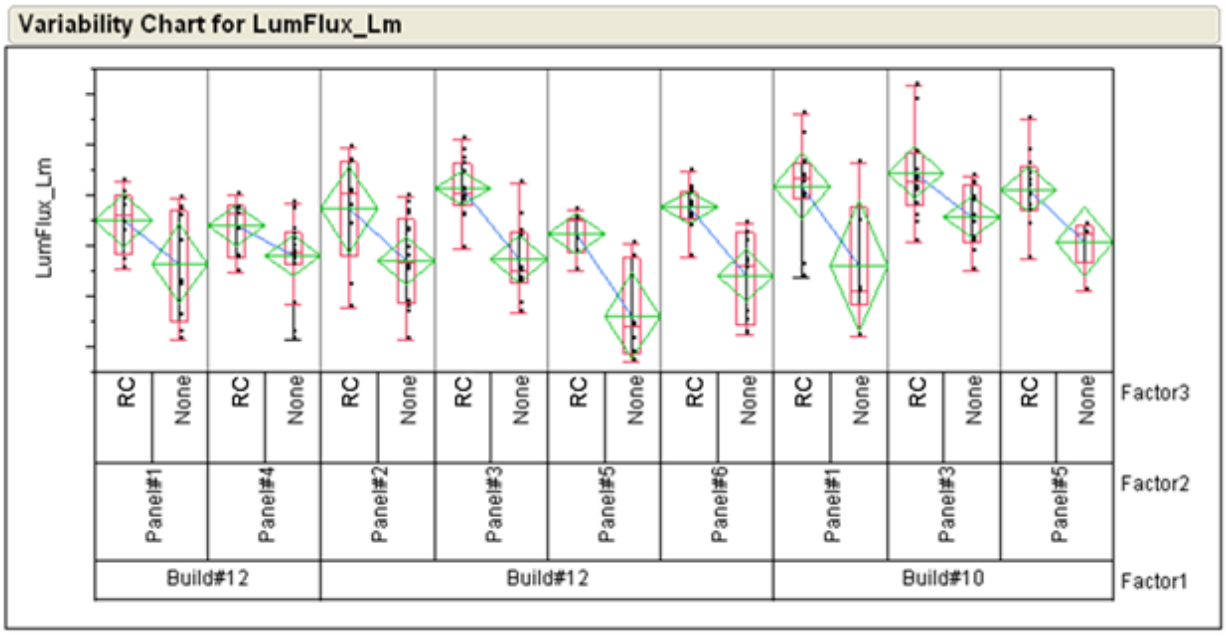

Fig. 19. Luminous flux for a number of fabrication lots, as measured in an integrating sphere. The abbreviation "RC" in the Factor3 field indicates packages containing a reflective substrate coating.

Small-footprint package

In the effort to minimize prototype package cost while maintaining efficacy, we designed a version of the lower-power package variant with a smaller footprint. This package was designed to accommodate various lower- and higher-power chip sizes and layouts. In addition, the primary optic design was appropriately scaled down such that the far-field emission would not differ appreciably from the current version. We anticipated that this new package version could reduce substrate and silicone lens costs by more than 30%. For evaluation purposes we specified two small-chip layouts: one in which the chips lay side by side, and the other in which the chip centers were offset to the maximum amount allowed by the smaller footprint, in order to establish the effect on package efficacy and far-field emission characteristics. The inter-chip spacing (perpendicular to the offset direction) was the same in both cases.

Package fabrication steps (chip placement, solder re-flow, phosphor application, and silicone lens application) of the new smaller prototype package did not differ significantly from the established larger package, with the exception of dicing for package singulation which utilized narrower blades due to the closer inter-package spacing. This spacing required some process development with respect to dicing alignment in order to avoid impinging too closely to the chips for some packages in the array. As performed previously, we explored different lens aspect ratios (height to width) to establish the effect of this parameter on efficacy and far-field emission. While we were seeking to minimize lens aspect ratio to reduce silicone lens cost, this could not come at the expense of efficacy or desirably broad far-field emission. Instant-on luminous flux (LF) measurements for differing aspect ratios and chip configurations are shown in Fig. 20. For the lens aspect ratios and chip configurations tested, LF did not vary appreciably. This was encouraging from a process stability standpoint, since variations in these geometric factors could presumably be tolerated with respect to LED output power.

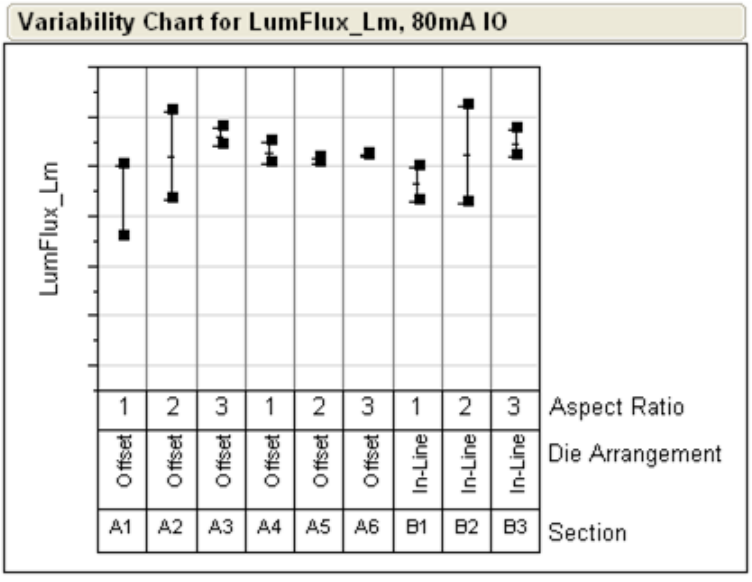

Fig. 20. Luminous flux of small-footprint prototype packages with varying lens aspect ratio and die arrangement as measured in a calibrated integrating sphere. Neither parameter appeared to significantly affect the net luminous flux.

As was previously done for the 'baseline' sized prototype package, the luminous flux values of numerous small-footprint packages were measured in comparison to a conventional Cree domed package, to verify that its optical efficiency (and therefore net package efficacy) was not inferior due to its non-standard geometry. To this end, packages with the standard domed lens and footprint but containing the smaller chips of the small-footprint prototype package were fabricated for comparison.

The color point and color rendering index (CRI) of all packages were verified to be in the same range (see Fig. 21), making comparison among them valid. As shown in Fig. 22, it was found that the small-footprint packages had a comparable luminous output to the baseline prototype packages as well as the domed package. This indicated that the novel lens geometry of the prototype packages was scalable, and did not suffer in optical efficiency relative to hemispherical lens packages despite its wider far-field emission distribution.

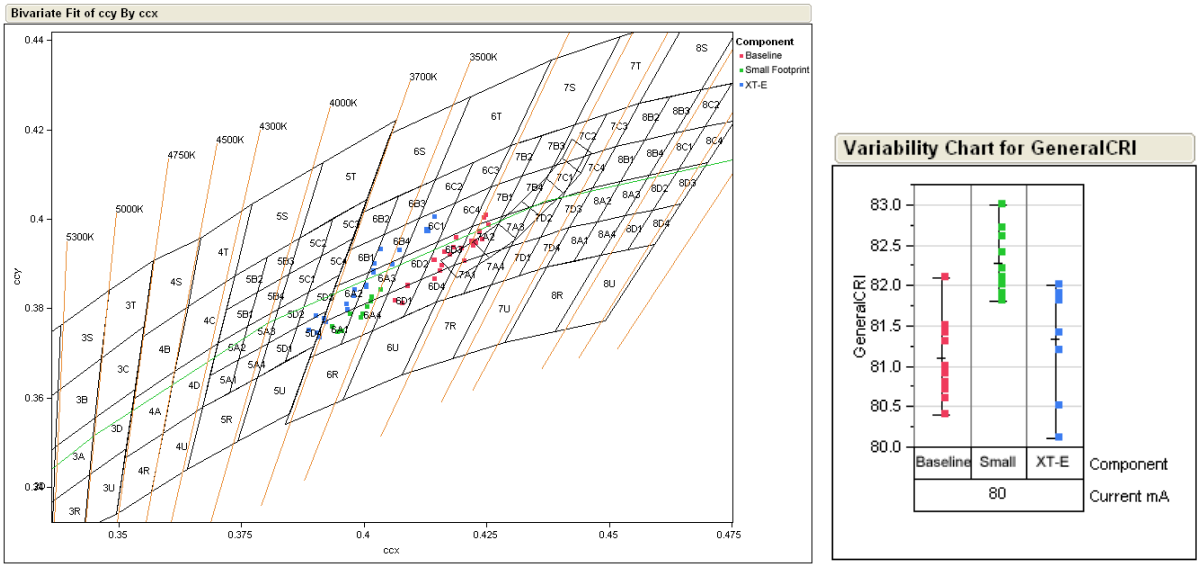

Fig. 21. Left: color points of small-footprint prototype packages plotted alongside baseline prototype packages and the standard domed package. Right: CRI values the three package types (baseline prototype, small-footprint prototype, and domed).

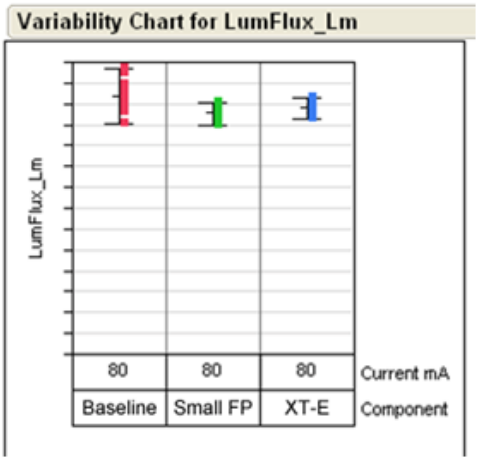

Fig. 22. Luminous flux vs. package type, showing that all average LF values were comparable at this representative drive current.

Having demonstrated efficacy on par with conventional domed packages, multiple repeat builds of the small-footprint package were performed to establish process reproducibility. Several of these builds were selected for package-by-package luminous flux and color point measurement in a calibrated integrating sphere. The results are shown in Fig. 23, with color points among these builds fairly consistent around the black body locus at ~3500K. Luminous flux values were also fairly tightly distributed. Although build 14 packages exhibited lower flux on average, these packages also contained blue chips with lower average radiant flux.

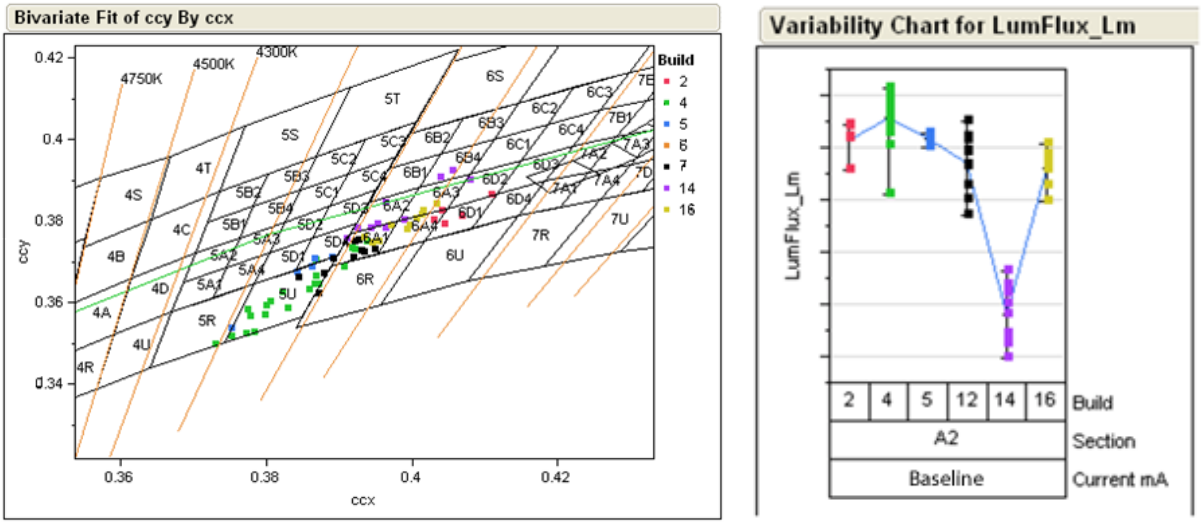

Fig. 23. Left: color points of numerous small-footprint prototype package builds, roughly centered about the black body locus at ~3500K. Right: luminous flux values for selected samples.

Accelerated lifetime testing runs of several lots of the small-footprint package were conducted in Cree's standard high-temperature and high-temperature/high-humidity conditions to determine if the new design has any unforeseen long-term reliability issues. As shown in Fig. 24, after more than 2,000 hrs. testing in HT/HH conditions the packages exhibited little change in luminous flux or color point. Therefore their operation under more moderate intended operating conditions in the troffer luminaire should yield a very long fixture lifetime.

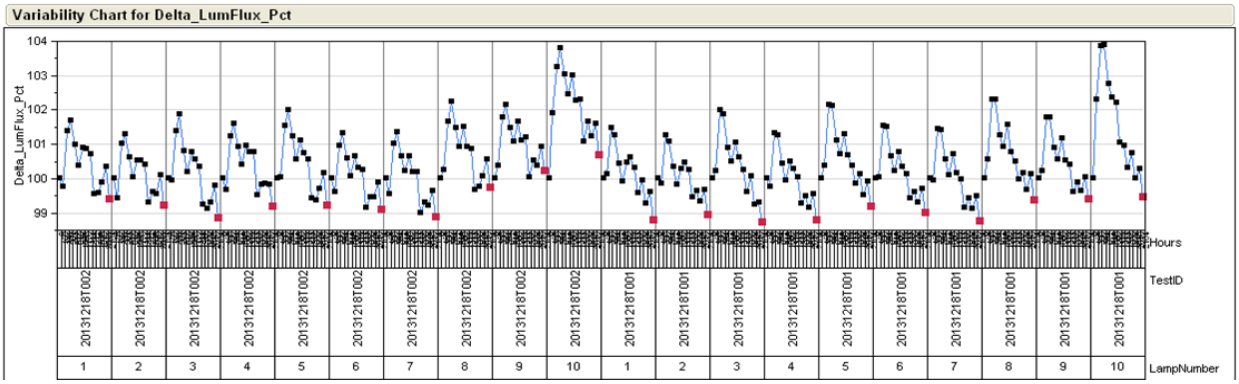

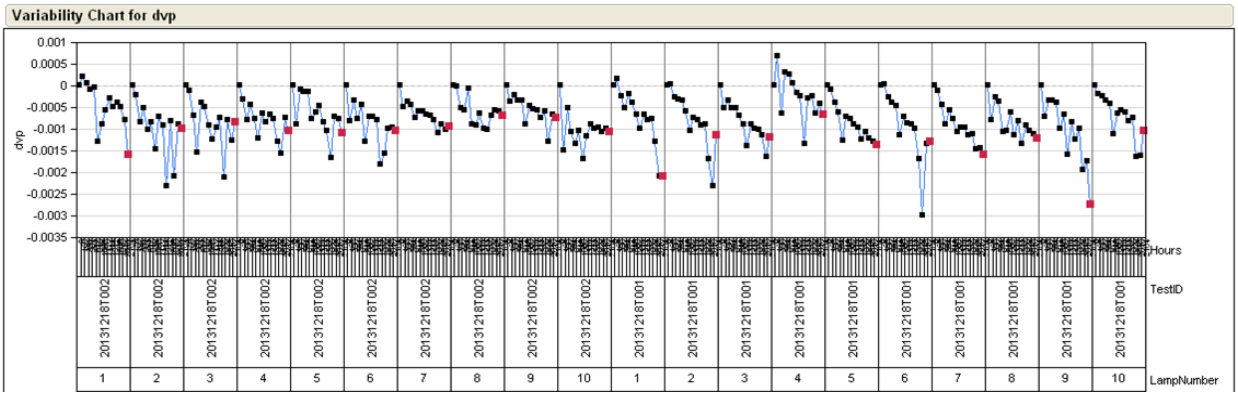

Fig. 24. Top: relative luminous flux of small-footprint prototype packages in high-temperature/high-humidity testing conditions at 2,184 hrs. Bottom: absolute color point shift (Δv') under the same conditions.

After an initial process development and test build, a new panel array of small-footprint LEDs was fabricated with several chip layout configurations and aspect ratios. The color rendering index (CRI) among all chip configuration and lens aspect ratios was consistent (see Fig. 25), thereby facilitating luminous flux (LF) comparisons among the various combinations.

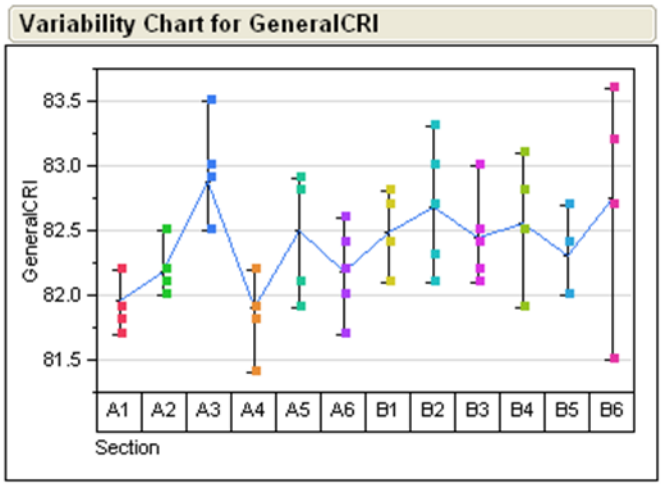

Fig. 25. CRI of the various small-footprint package configurations, in which chip arrangement and primary optics aspect ratios were varied. The average CRI of the various combinations did not differ significantly, thereby simplifying LF (and efficacy) comparisons among them.

We also confirmed the color point consistency of this newer LED build, which as shown in Fig. 26 was well controlled and did not vary appreciably with changes in chip configuration or lens aspect ratio. The LF (and therefore efficacy) of the package configurations could thus be compared without the need for adjustment due to differing color point.

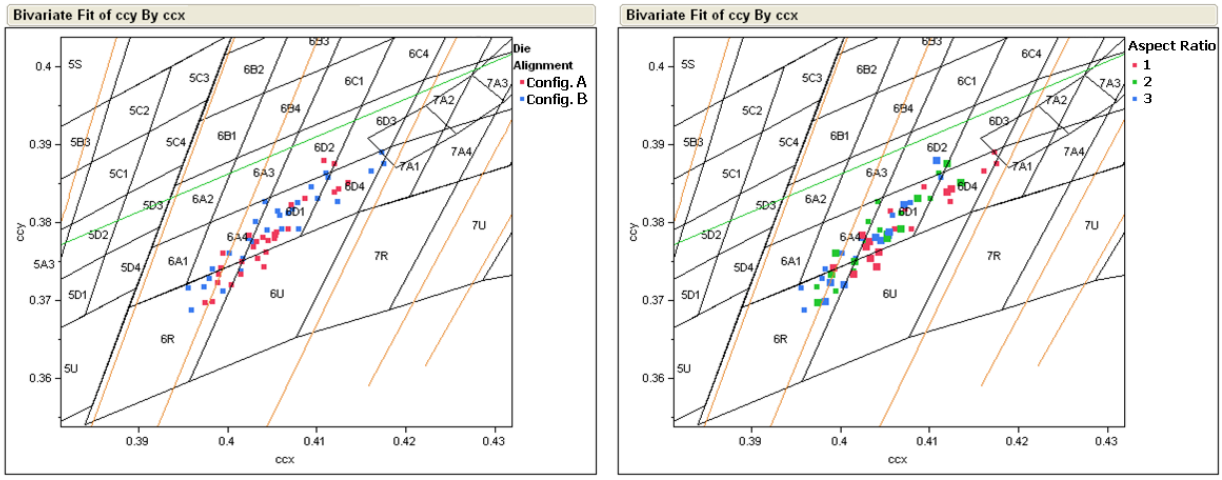

Fig. 26. Color point of small-footprint prototype package builds, based on changes in chip configuration (left) and lens aspect ratio (right). The color point consistency was high for both cases, eliminating the need for corrections in measured LF (and therefore efficacy).

Prototype packages with varying combinations of chip configuration and lens aspect ratio were fabricated simultaneously on the same panel with sorted blue-emitting dies to ensure consistency. The room-temperature, instant-on efficacy values of these packages were quantified in an integrating sphere, with results shown in Fig. 27. The efficacy of packages with chip layout B was lower in all cases, and fell slightly as lens aspect ratio was increased.

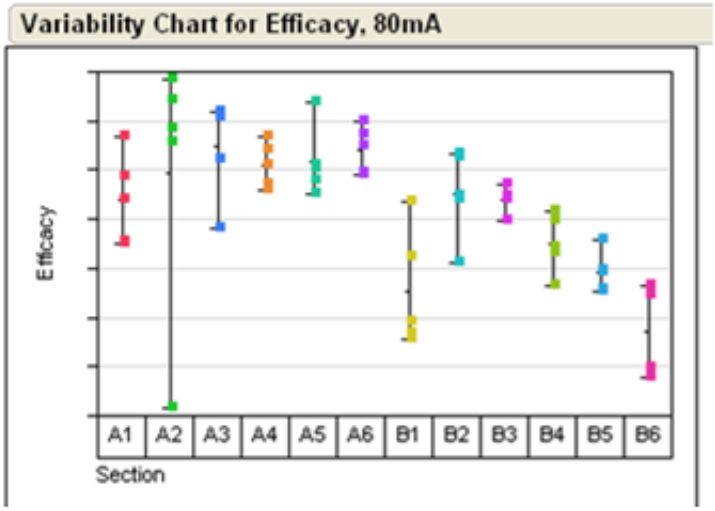

Fig. 27. Relative efficacy of various combinations of chip layout and lens aspect ratio for the small-footprint prototype package. The efficacy of packages with chip layout B was lower in all cases, and fell slightly as lens aspect ratio was increased.

A key part of the efficacy evaluation of the small-footprint prototype packages was comparison to the established larger-footprint version. This was done at the same color point and CRI to avoid the need for corrections, as discussed above. In Fig. 28 it is evident that the total variation in color point was comparable between the two package sizes, making comparison straightforward.

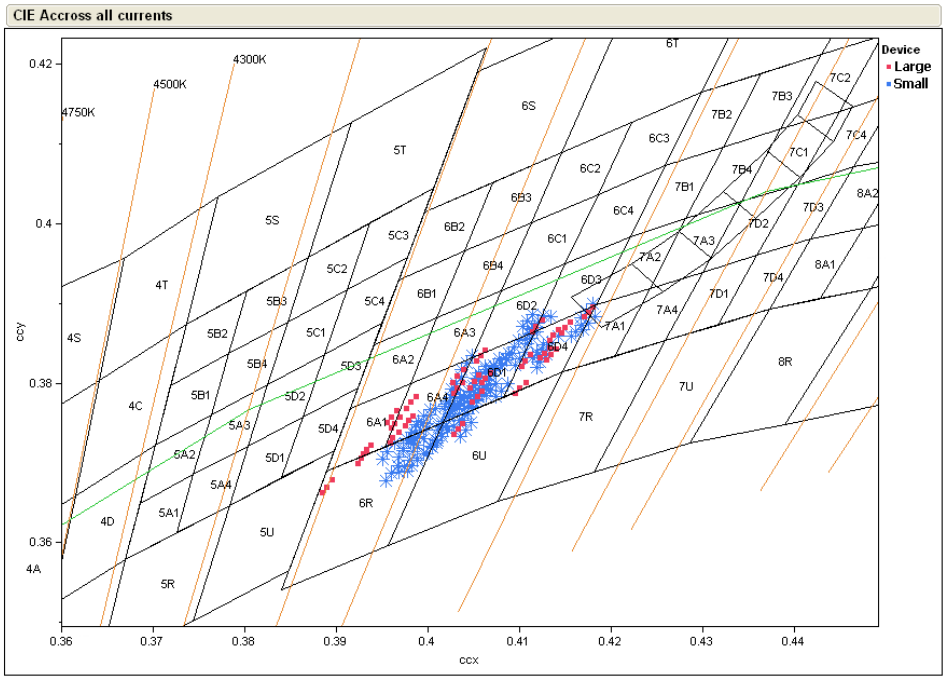

Fig. 7. Color point (plotted as CIE CCx, CCy) of small-footprint vs. larger-footprint prototype packages. The color point consistency was sufficient to eliminate the need for corrections in measured LF (and therefore efficacy).

The efficacy of the various small-footprint package configurations emitting at 82-83 CRI and ~3000K CCT is compared with five batches of corresponding large-footprint packages in Fig. 29. We found that the average efficacy of the small-footprint packages with chip configuration A was slightly lower than the efficacy of their larger-footprint counterparts..

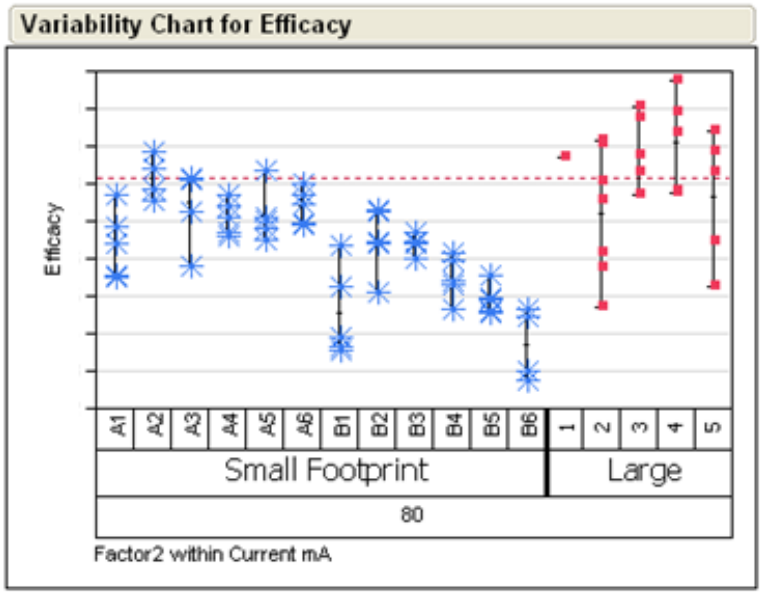

Fig. 29. Relative efficacy comparison at 82-83 CRI and 3000K CCT of small-footprint prototype packages (left) with previously developed large-footprint packages (right). The red dashed line indicates the overall average efficacy for the larger footprint version.

Integrated TrueWhite Prototype Packages

Based on our experience in fabricating variants of the prototype package, we began work on a version that incorporated Cree's TrueWhite® (TW) approach, *i.e.* the use of blue chips coated by a yellow phosphor in tandem with direct red-emitting chips. Cree has utilized this approach using discrete LEDs in commercial systems which simultaneously achieve high CRI and high efficacy, since red chips are much more efficacious than conventional red phosphors. In an integrated TrueWhite® package phosphor-coated blue chips are placed side-by-side with red chips. The advantage should be enhanced blue/yellow/red color mixing at the package level, reducing the need for such mixing by secondary optics in the system. However, we also had to consider the challenges of blue and yellow light absorption by the red chips, as well as methods to selectively apply phosphor to only the blue chips.

As an analog of the lower- and higher-power prototype packages developed previously, we designed versions of the TW package which varied the number of blue and red chips to establish the effect on efficacy and far-field color uniformity, among other metrics. Initial layouts were designated based on the number of blue/yellow and red chips. During preliminary selective phosphor application trials (Fig. 30) we found that there was some undesirable overlap of the phosphor onto the red chips, which could result in uncontrolled scattering or even absorption. In addition, 'drifting' (excess buildup) of phosphor was occasionally observed on the blue chips, which is undesirable since significant color point variation could occur. Process development and tooling modifications were undertaken to overcome these challenges in the selective phosphor application, with an emphasis on keeping the process practical for scaled production.

Fig. 30. Micrographs of challenges encountered during initial trials of selective phosphor application. Left: overlap with red chip positions; center: pile-up of phosphor on blue chips; right: phosphor buildup on red chip wire bonds.

Initial challenges in selective phosphor application were overcome, such that minimal phosphor was inadvertently applied to the red chips in the package. Subsequent work focused on the number, size, and configuration of blue and red chips in the package, since it was anticipated that some blue and yellow light could be absorbed by the red chips, which could partially counteract the advantage of using red chips instead of red phosphors.

A number of different blue and red chip configurations were built and tested. Since an input current density (*e.g.* A/cm^2) was difficult to define when simultaneously driving blue and red chips, we instead calculated the equivalent total input power density by dividing combined input power by combined chip area. The results are summarized in Fig. 31, in which the relative efficacy values of various TW configurations were compared with low- and high-power 'baseline' (blue + phosphor) versions of the prototype package. For TW packages, the blue- and

red-chip current were tuned for each configuration to bring the color point onto the black-body locus at ~3500K.

As evident in Fig. 31, at nearly all input power density levels the efficacy of one or more of the TW configurations was higher than both the "high power" and "low-power" chip + phosphor packages. The "A" and "D" layouts in particular had stand-out efficacy values, which were attributed to the minimized red chip area in these packages. This was confirmed by independently testing the efficacy of just the blue + phosphor string for each TW package at a single current. It was evident that for a given number of blue chips, the number (and therefore total area) of red chips should be minimized to correspondingly diminish blue/yellow light absorption.

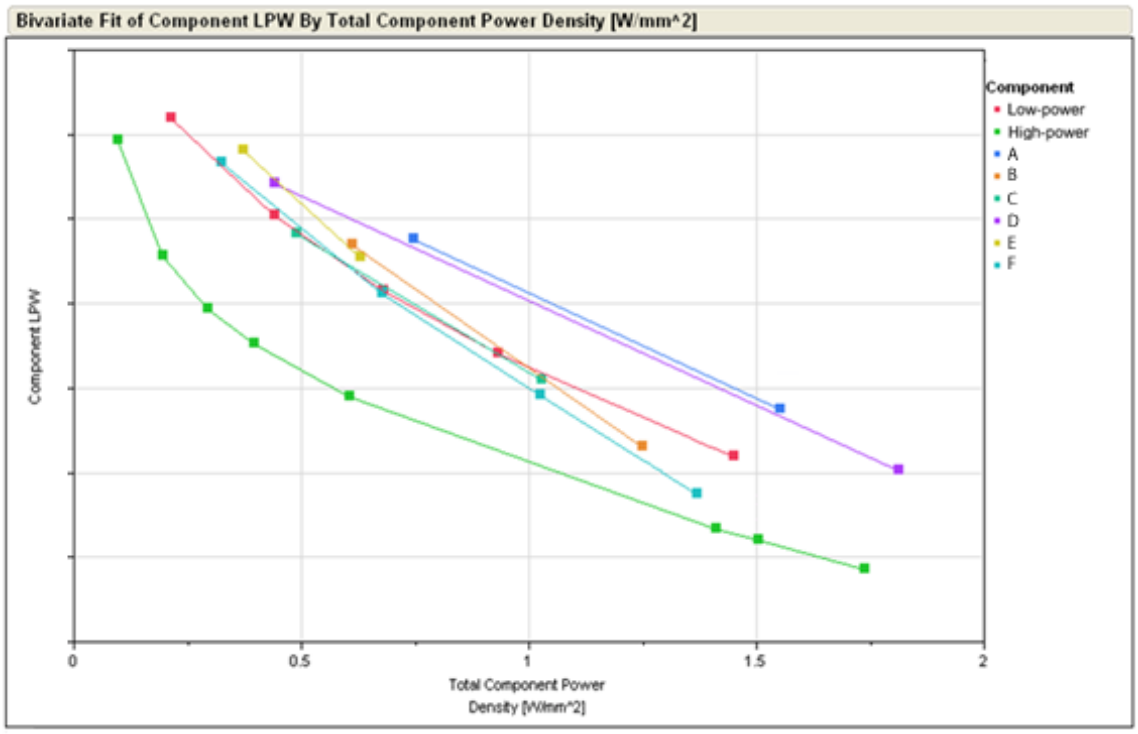

Fig. 31. Instant-on LED component efficacy (lm/W) vs. input power density for a variety of prototype TW (A-F) and blue+phosphor configurations ("low power" and "high power"). The TW configurations had higher efficacy at nearly all input power density levels.

Task 2.2 – Board Integration

With the prototype package geometry having been defined, we anticipated that the packages would be driven at an input electrical power of 0.25 – 1.0W (depending on intra-package chip configuration). This provided an input for thermal modeling of packages placed in the system.

We modeled prototype packages on conventional fiberglass-reinforced epoxy laminate printed circuit board (FR-PCB), a low-cost baseline platform that can be readily measured for verification. Using representative values for parameters such as package thermal resistance, FR-PCB thickness, copper trace thickness and gap width, the LED junction temperature (T_j) for individual LED packages on free-standing FR-PCB (in air, with no heat sink) was simulated. This was an intentionally conservative case (*e.g.* compared to PCB on metal) in which the

simulated T_j should be higher than would be observed in an actual system where the PCB is in direct contact with the troffer enclosure, for instance. The T_j of individual prototype packages at 1W input electrical power is shown for two example configurations in Fig. 32, which in addition to simulations of LED arrays will serve as basic test cases for experimental validation.

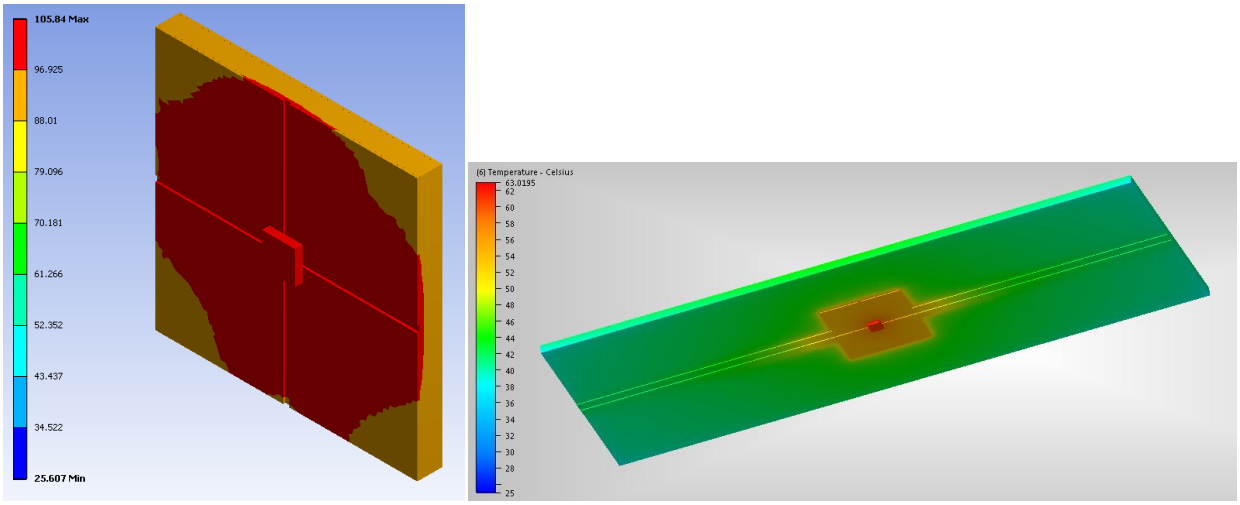

Fig. 32. Simulated thermal profiles of prototype packages (depicted as square elements) on 1mm thick FR-PCB with lateral sizes of 0.5 x 0.5" (left) and 3 x 1" (right). The estimated junction temperatures are 106°C and 63°C, respectively, illustrating the important effect of PCB dimensions on LED T_j.

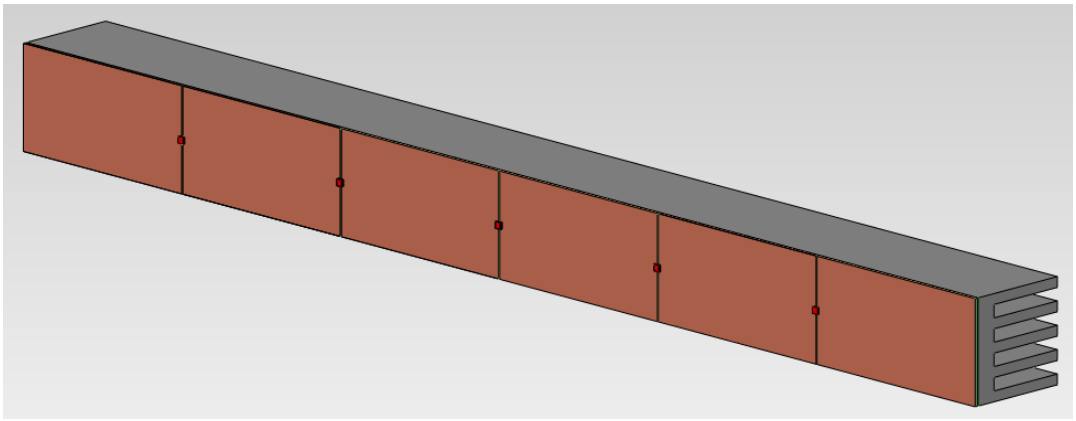

Fig. 33. Schematic of a thermal simulation case with prototype LEDs (depicted as red squares) arrayed at 2" intervals on a 1" wide FR-PCB (thin green plane) mounted to a heat sink (gray). The copper trace covered most of the FR-PCB face.

Using representative estimates for parameters such as package thermal resistance, FR-PCB thickness and width (1"), copper trace thickness and gap width, the junction temperature (T_j) for LED packages in arrays on a free-standing FR-PCB (in air, with no heat sink) was compared with those on an FR-PCB in contact with a heat sink. An example configuration of the latter configuration is depicted in Fig. 33. Input electrical power values of 0.25 and 1.0 W were compared at various inter-package spacings, as summarized in Fig. 34. The effect of the heat sink on T_j was more pronounced for the higher input power at closer LED spacings, which

indicated the limitations that the thin copper trace and the FR-PCB itself have in conveying heat away from the LEDs. It was encouraging that nearly all combinations of input power and LED spacing yielded T_j values acceptable for sustained LED operation, which we provisionally set at $\leq$ 85°C. Further simulations focused on the effect of copper trace dimensions (*e.g.* thickness, width, LED pad size), since much of the heat extraction from the LEDs is facilitated by this thin metallic layer. We sought to minimize copper trace area and thickness (and therefore cost), while understanding the trade-offs of such minimization with overall thermal management.

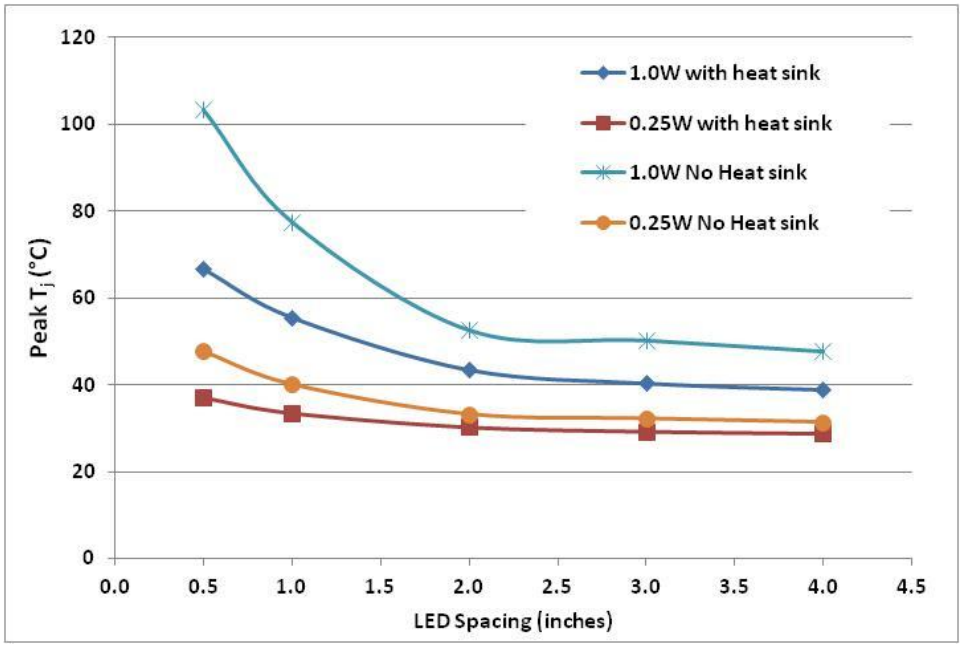

Fig. 34. Maximum simulated junction temperature (T_j) vs. LED spacing for 0.25W and 1W input power, each with and without a heat sink backing the 1" wide FR-PCB. Nearly all combinations yield a T_j lower than 85°C.

To establish the feasibility of attaching large numbers of arrayed prototype LED components to PCBs within the troffer luminaire, we conducted a large number of package attach (solder reflow) procedures and quantified the yield via electrical measurements. Solder paste was simultaneously and selectively applied to all LED positions using a stencil masking process in a manner consistent with production methods. Prototype packages were located on circuit boards using automated "pick & place" equipment in a close approximation to methods used in production. A solder reflow temperature cycle firmly attached the packages to the boards, and electrical and optical testing was carried out to confirm that packages were properly attached. As shown in Fig. 35, this testing resulted in a component attach yield of 99.0%, which was promising for the large-scale distribution of prototype LEDs in troffer luminaires. All components except for one exhibited forward voltage and luminous flux values in expected ranges. This yield result demonstrated that for our current prototype LED package geometry, component attach to printed circuit board materials was reliable.

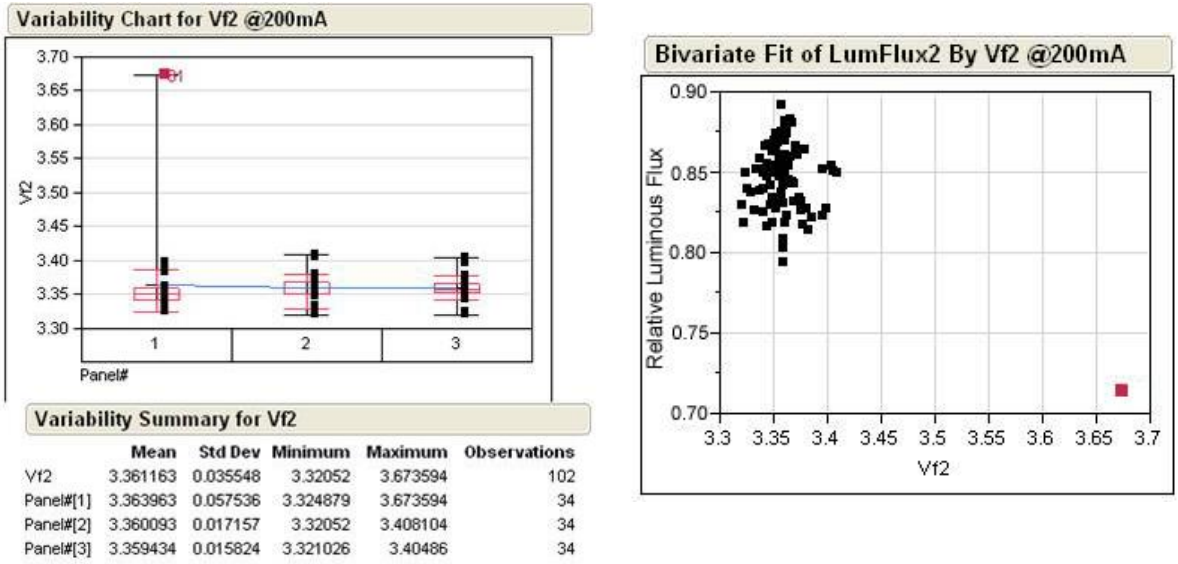

Variability Summary for Vf2

	Mean	Std Dev	Minimum	Maximum	Observations
Vf2	3.361163	0.035548	3.32052	3.673594	102
Panel#[1]	3.363963	0.057536	3.324879	3.673594	34
Panel#[2]	3.360093	0.017157	3.32052	3.408104	34
Panel#[3]	3.359434	0.015824	3.321026	3.40486	34

Fig. 35. Left: forward voltage of prototype LEDs solder-attached to PCBs. Right: Relative luminous flux vs. forward voltage. All components except for one conformed to expect V_f and LF ranges.

In summary, via modeling and measurements it was found that at the anticipated LED operating current (and therefore input power), the rise in LED solder point temperature was well within acceptable package operating limits. Low (< 3%) thermal roll-off was observed when comparing instant-on to steady-state luminous flux of LED arrays. Therefore, we verified that this low-cost PCB platform was more than adequate for our performance requirements, and we did not need to consider higher-cost options such as metal-core PCBs and heat sinks.

Using thermal simulations and LED-on-board demonstration builds as guidance, we fabricated arrays of prototype LEDs (built to ~3500K CCT, 90+ CRI) on circuit boards and mounted them onto a steel panel to compose a prospective light engine. This light engine was tested "instant on" (momentarily at room temperature) and at steady state in an integrating sphere under anticipated drive current. The resulting color point for both conditions is shown in Fig. 36, which demonstrates that the color point did not change much as a result of LED heating. The net luminous flux, CRI, and efficacy of this prototype light engine are shown in Table 2. With a steady-state luminous flux of ~5300lm, this prototype exceeded the target set in the milestone "LED light engine providing with 5200 lumens at 3500K CCT and CRI of 90". In addition, the thermal roll-off (decrease in luminous flux due to self-heating at steady state relative to "instant on", *i.e.* room temperature) was ~4%, lower than the target of 6% set in the milestone "Fixture thermal roll-off (instant-on to steady state) at 6%." This thermal roll-off was consistent with earlier simulations and measurements, and demonstrated that no heat sinks were needed in the troffer.

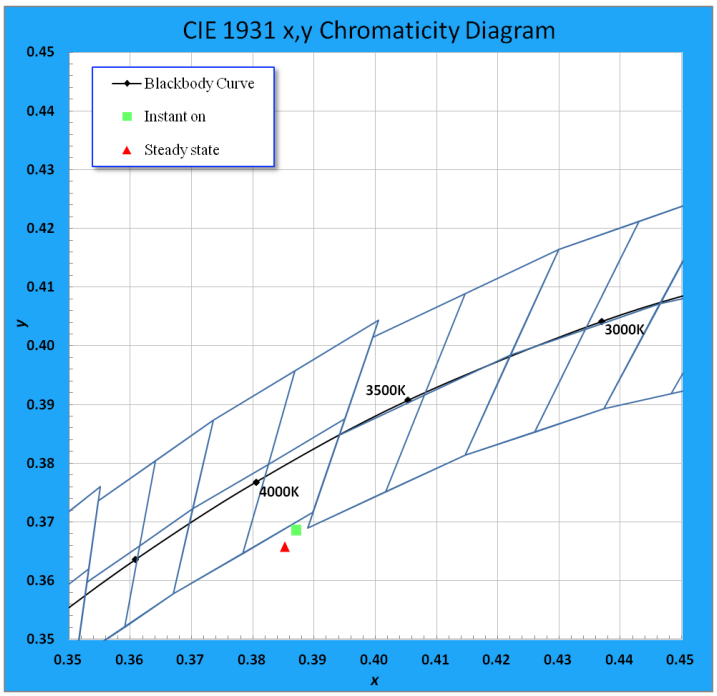

Fig. 36. Left: Photograph of the prototype light engine as tested in a 2m integrating sphere. Right: CIE x,y color points of the light engine under instant-on and steady-state test conditions.

Table 2. Luminous flux, color temperature, CRI and efficacy of a prototype troffer light engine tested "instant on" (instantaneously at room temperature) and at "steady state" (sustained operation with self-heating). The thermal roll-off in luminous flux was ~4.4%, lower than the milestone target of 6%.

Measurement Condition	**Luminous Flux** (lm)	**Color Temperature** (K)	**CRI**	**Efficacy** (lm/W)
Instant On	5555	3754	94.3	106.6
Steady State	5308 (**-4.4%**)	3782	93.6	104.6

Task 3 – Fixture Design and Development

Task 3.1 – Fixture Optical Design

The direct-view troffer design pursued during this project required an efficient, low-cost single-pass optical diffuser. Initial optical modeling indicated the potential for a few selected diffuser designs that would effectively homogenize intensity distribution without introducing too much optical loss. Our aim was to utilize a light diffusion scheme with lower than 10% system optical loss. We investigated several combinations of prototype LED spacing and LED-to-diffuser distance in a scaled-down fixture to evaluate whether any visible "pixelation" (perceptible luminance variation) was evident. Pixelation is a qualitative metric based upon feedback from a sampling of observers within our development group.

A representative data set is shown in Fig. 37 for four diffuser designs with increasing

nominal diffusion angle. In this plot, an LED spacing below the data point at each given diffuser height was considered "acceptable". As is evident from these data, optimal combinations of LED spacing and LED-to-diffuser height varied considerably depending on diffuser design (diffusion angle and transparency). The shaded green area indicates a tentatively developed zone of favorable combinations of LED spacing and diffuser height, which took into account LED cost, diffuser cost, and required total lumen output.

Although it was obviously desirable from a cost standpoint to maximize inter-LED spacing (at a given overall luminous flux requirement) and minimize troffer height, this approach was limited by the dual constraints of tolerable pixelation and optical loss. Diffusers with higher nominal diffusion angle may be advantageous in providing homogenized luminance, but they could introduce increased optical loss via multiple light bounces within the enclosure.

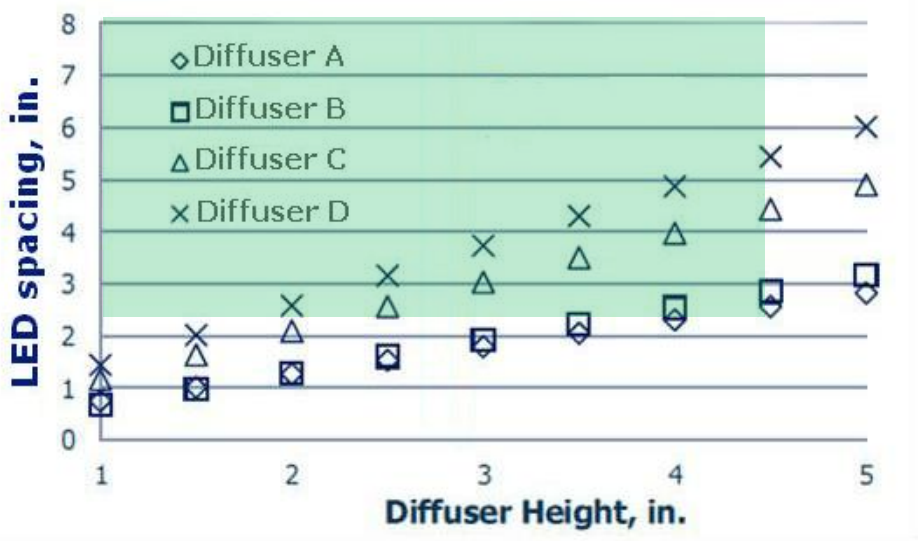

Fig. 37. Comparison of observed pixelation at various combinations of LED spacing and LED-diffuser distance for four diffuser designs. The data points mark the maximum LED spacing at which pixelation is not discernible. The shaded green area represents an evaluation of desirable combinations of LED spacing and diffuser height.

We constructed two small-scale test beds in which an array of prototype LEDs could be housed, and on top of which diffusers were placed to evaluate their optical loss. These test beds, 6x6" in lateral size with depths of 1" and 2", had internal surfaces covered with highly reflective Lambertian white paper to approximate the reflective surfaces that were likely to be used in our final demonstration troffer.

We evaluated two diffuser designs (Type 1, Type 2) with various nominal diffusion angle values by comparing the luminous flux in a 1m integrating sphere with and without each diffuser in place. The ratio of the former to the latter indicates the optical loss due to light being absorbed within the diffuser or within the test bed after being back-scattered by the diffuser. Results shown in Fig. 38 indicated that most of the diffuser variants tested passed the < 10% optical loss requirement, and that the two diffuser types did not differ significantly from one another. Since net optical loss is a function of not just the diffuser but the interplay of scattering and absorption among diffuser and fixture surfaces, future testing was also conducted on larger fixture test beds with a higher aspect ratio between lateral to vertical size. This indicated the 'scaling' of system optical loss with a given diffuser design, if any.

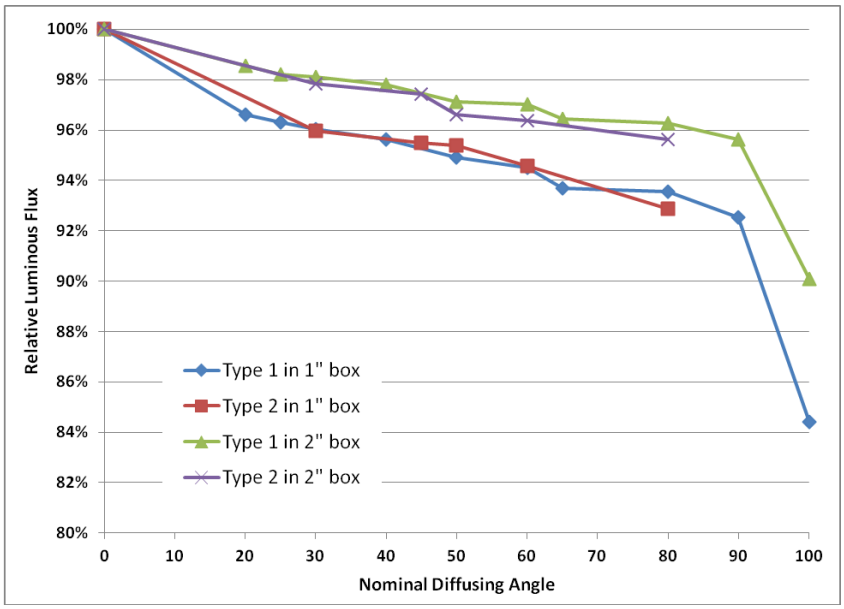

Fig. 38. left: Relative luminous flux vs. nominal diffusing angle (in degrees) for two diffuser types as measured in an integrating sphere on 1" and 2" deep test beds. Note that the points at 0° are for no diffuser. right: a photograph of the 2" deep test bed in the integrating sphere.

The results above were for relatively thin (< 1mm) diffusers, which may not have been sufficiently structurally robust to span large areas in the final demonstration luminaire. We therefore obtained diffuser panels of higher thickness with two different nominal diffusion angles, to establish the effect of thickness on system optical efficiency. While higher diffuser thicknesses are desirable to minimize diffuser sheet bowing under its own weight, the higher cost of these thicknesses must also be considered.

We measured the relative luminous flux (an indicator of system optical efficiency) of the 1" and 2" deep test beds with diffusers of varying thickness at a two nominal diffusion angles. As shown in Fig. 39, the relative flux of the 40° diffusion angle samples dropped by less than 4% for the thickest (6mm) sample, and by up to ~6% for diffusers with 80° nominal angle. In both cases, the approximate net system optical efficiency was greater than our target of 90%, and the relative flux at each thickness did not differ appreciably between the two diffusion angle values. The non-monotonic decrease of relative LF vs. thickness for the 80° samples may have been a measurement artifact: the 3 and 6mm thick diffuser panels had more exposed edge area as they sat on the diffuser test beds. Waveguided (channeled) light, expected to be higher for a 80° diffusion angle than the 40° case, could then escape from these exposed edges.

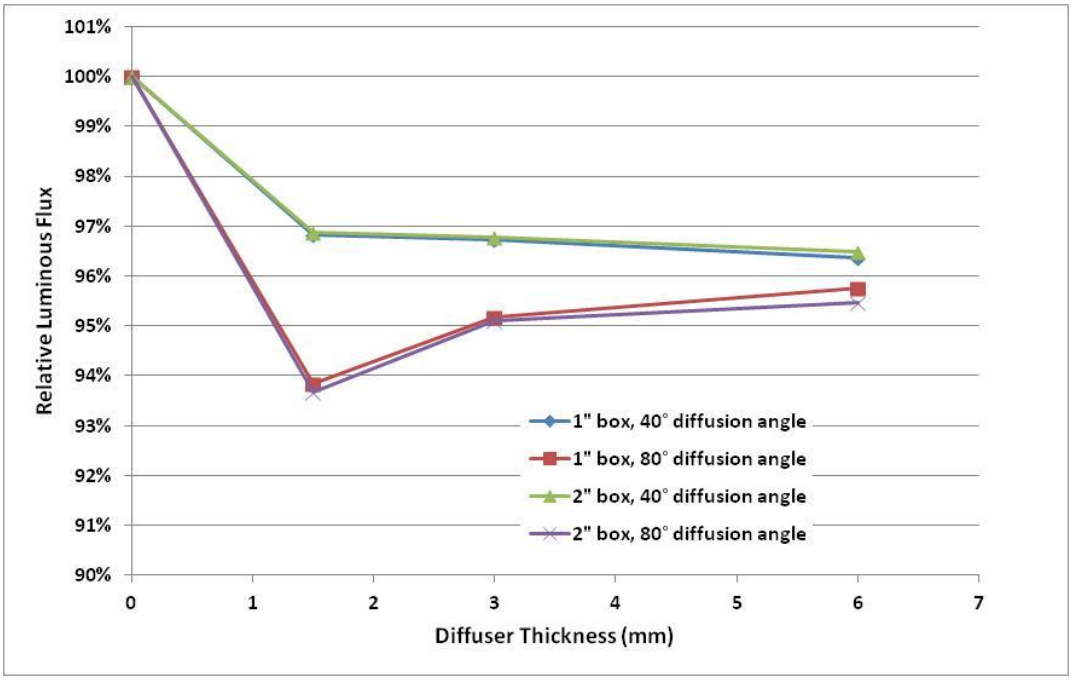

Fig. 39. Relative Luminous flux vs. diffuser thickness for two nominal diffusion angle values. The luminous flux relative to an open test bed dropped by as much as 6%, which still yielded a system optical efficiency higher than our target of 90%.

When measuring luminous flux change vs. diffuser thickness we also considered color point shifts that the diffusers could induce, whether on their own (*e.g.* preferential absorption of certain wavelengths within the diffuser), and also in combination with light scattered from the surfaces within the test bed. As shown in Fig. 40, we found that color point indeed changed when diffusers were put in place, with the 80° designs exhibiting larger shifts. With shifts as large as 0.0017 in CCx and 0.0016 in CCy (for the 1.5mm thick 80° diffusion angle), it was likely that to reach a desired color point for the final demonstration troffer, we would need to correspondingly modify of the color point of the prototype LEDs via adjustments to phosphor composition and/or application thickness. This is a straightforward requirement and should not complicate LED fabrication.

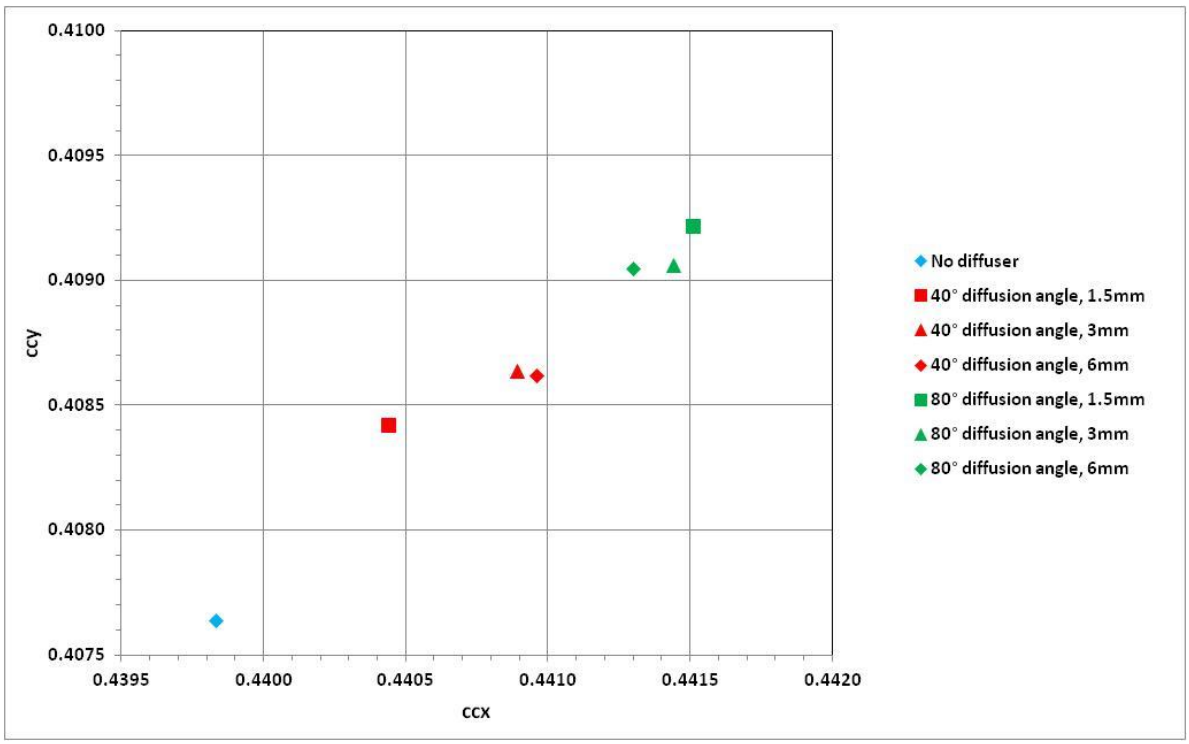

Fig. 40. Color coordinates (CCx, CCy) of light emitted from the 1" deep test bed for various combinations of nominal diffusion angle and diffuser thickness. Both 40° and 80° designs exhibited significant color shifts, with the latter showing larger changes. The largest shift observed was 0.0017 in CCx and 0.0016 in CCy, which could be compensated for via modification of the LED color point, if necessary.

We previously measured relative luminous flux (an indicator of system optical efficiency) of our 1" and 2" deep diffuser test beds with diffusers of varying thickness at two nominal diffusion angles. The non-monotonic decrease observed for relative LF vs. thickness for the 80° diffuser samples was suspected to have been a measurement artifact, since waveguided (channeled) light could escape from exposed diffuser edges. We performed this measurement series again with diffuser edges masked by reflective white paper in order to minimize light escape from these surfaces. The result is shown in Fig. 41, in which the luminous flux relative to the no-diffuser case is plotted vs. diffuser thickness for two nominal diffusion angles. The 40° diffusion angle design exhibited a monotonic decrease in relative flux (and therefore system optical efficiency) vs. thickness, whereas the 80° diffusion angle showed a dip in relative flux at a diffuser thickness of 1.5mm, similar to what had been observed previously. The subsequent slight recovery in relative LF with diffuser thickness is therefore not a result of light leakage from diffuser plate edges, but apparently due to the interplay of light scattered at this higher diffusion angle within a higher plate thickness. Likewise, the color point shifts induced by thick diffusers did not vary signficantly between masked and non-masked diffuser plate edges.

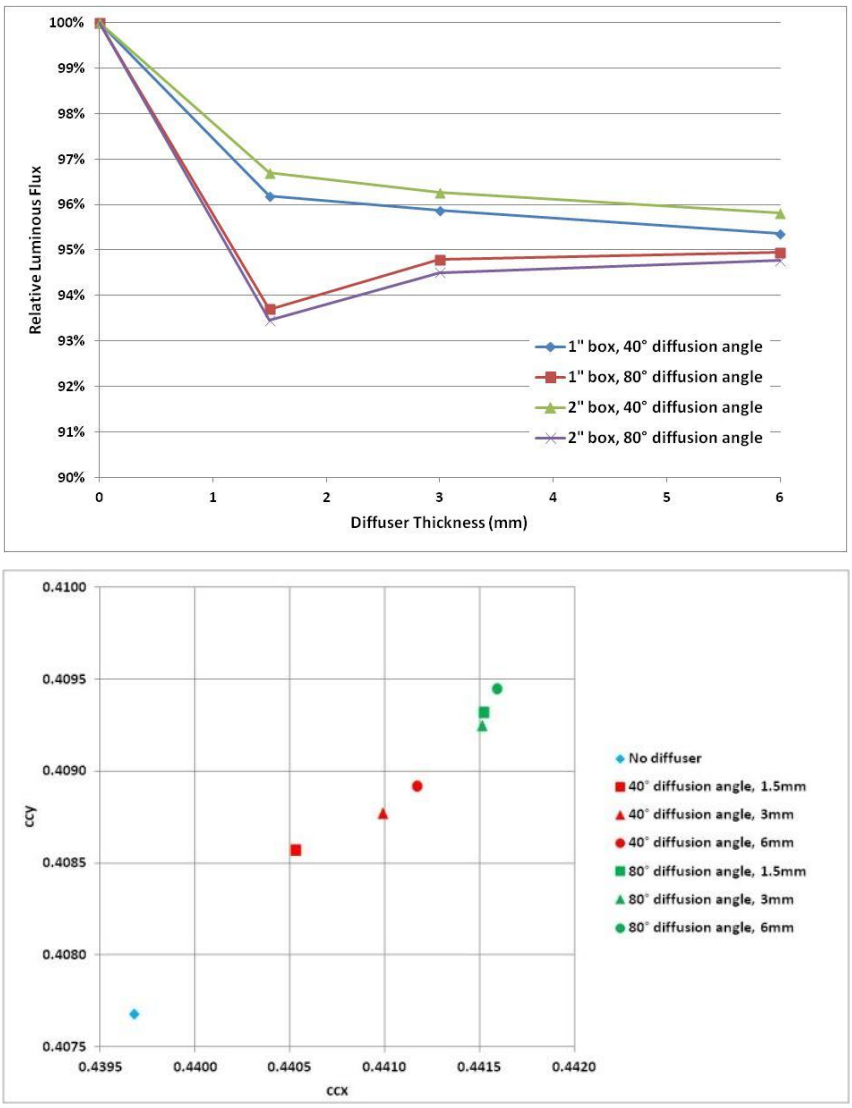

Fig. 41. Left: Relative luminous flux (an indicator of system optical efficiency) vs. diffuser thickness for diffuser plates with masked edges. Left: the color coordinates of each diffuser type/thickness plotted in cc_x/cc_y color space. The LF and color point values of these masked-edge diffusers is comparable to the un-masked versions.

By analyzing the numerous diffuser measurement studies we conducted, we established the interplay among parameters such as inter-LED spacing, LED-to-diffuser spacing, diffuser material, nominal diffusion angle, and diffuser thickness. The resulting data sets acted as guidance in the design space for the diffuser used in our final demonstration troffer luminaire.

We have established the interplay among parameters such as inter-LED spacing, LED-to-diffuser spacing, diffuser material, nominal diffusion angle, and diffuser thickness. While optical efficiency of the diffusers is readily quantifiable in an integrating sphere, up to this point we had qualitatively evaluated characteristics such as diffuser luminance uniformity (*e.g.* perceptible LED "pixelation").

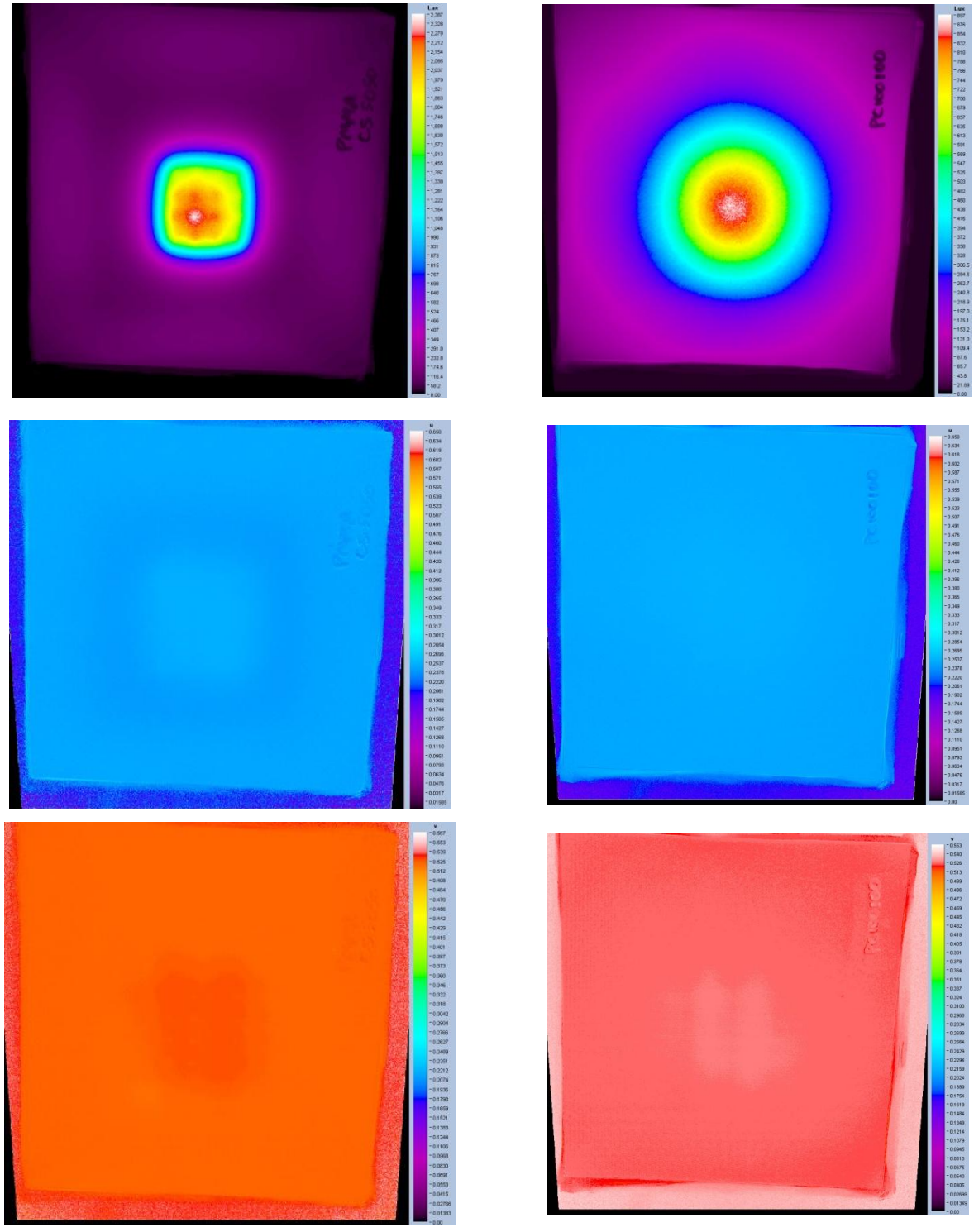

Fig. 42. Illuminance (top row) and color point (u': middle row, v': bottom row) images for diffusers with 50° (left) and 100° (right) diffusion angles on a 1" test bed with prototype LEDs spaced in a ~1cm array. Note the differing luminance scales: 2387 lux at right and 897 lux at left, indicating much larger luminance variation of the 50° diffuser.

In an effort to make this evaluation more quantitative, we began using an imaging colorimeter with a 1024x1024 pixel array. By correlating qualitative and quantitative color and luminance measurements, we worked to establish reproducible variation acceptability criteria for this and other luminaire form factors. An example is shown in Fig. 42, in which diffusers were placed on a 1" deep diffuser test bed with an array of prototype LEDs with ~1 cm spacing (*i.e.*, a demanding combination of intra-LED spacing and LED-diffuser separation). Diffusers with 50° vs. 100° nominal diffusion angle exhibit quite different color point and luminance variation vs. position, which agreed with qualitative evaluation by eye.

We periodically evaluated candidate optical diffuser designs with respect to spacing among prototype packages, and from the packages to the diffuser surface. For a highly reflective cavity (97-98% white paper was typically used), the optical efficiency of scaled-down luminaires was higher than our target of 90%. While evaluating optical efficiency in an integrating sphere, we of course also measured absolute luminous flux emitted from each configuration, and could therefore quantify the luminous flux per unit area. We found this method to more reproducible than using a hand-held luminance meter, since the integrating sphere collected nearly all light emitting from the luminaire, and was more consistent than attempting to position a meter at a given distance or angle from the luminaire. In Table 3 below we list examples of lm/in^2 values derived from integrating sphere measurements, all of which exceeded the milestone value of 20 lm/in^2.

Table 3. Luminous flux per unit area calculated from a 2-inch deep scaled-down troffer luminaire with representative LED drive current and inter-LED spacing.

Diffuser	Diffusion angle (°)	Diffuser thickness (mm)	Luminous flux (lm)	lm/in^2
None	None	0.0	1164.0	**36.4**
Mat. B	40	1.5	1125.6	**35.2**
Mat. B	40	3.0	1120.5	**35.0**
Mat. B	40	6.0	1115.3	**34.9**
Mat. B	80	1.5	1087.8	**34.0**
Mat. B	80	3.0	1100.1	**34.4**
Mat. B	80	6.0	1103.1	**34.5**

Task 3.2 – Thermal Design

Thermal modeling was largely focused on simulating prototype packages on conventional fiberglass-reinforced epoxy laminate printed circuit board (FR-PCB), a low-cost baseline platform that can be readily measured for verification. Using representative values for parameters such as package thermal resistance, FR-PCB thickness and width (1"), copper trace thickness and gap width, the LED junction temperature (T_j) for individual prototype LED packages on free-standing FR-PCB (in air, with no heat sink) was compared with those on a heat sink. Nearly all combinations of input power and LED spacing have yielded T_j values acceptable for sustained LED operation, which we set at $\leq 85°C$.

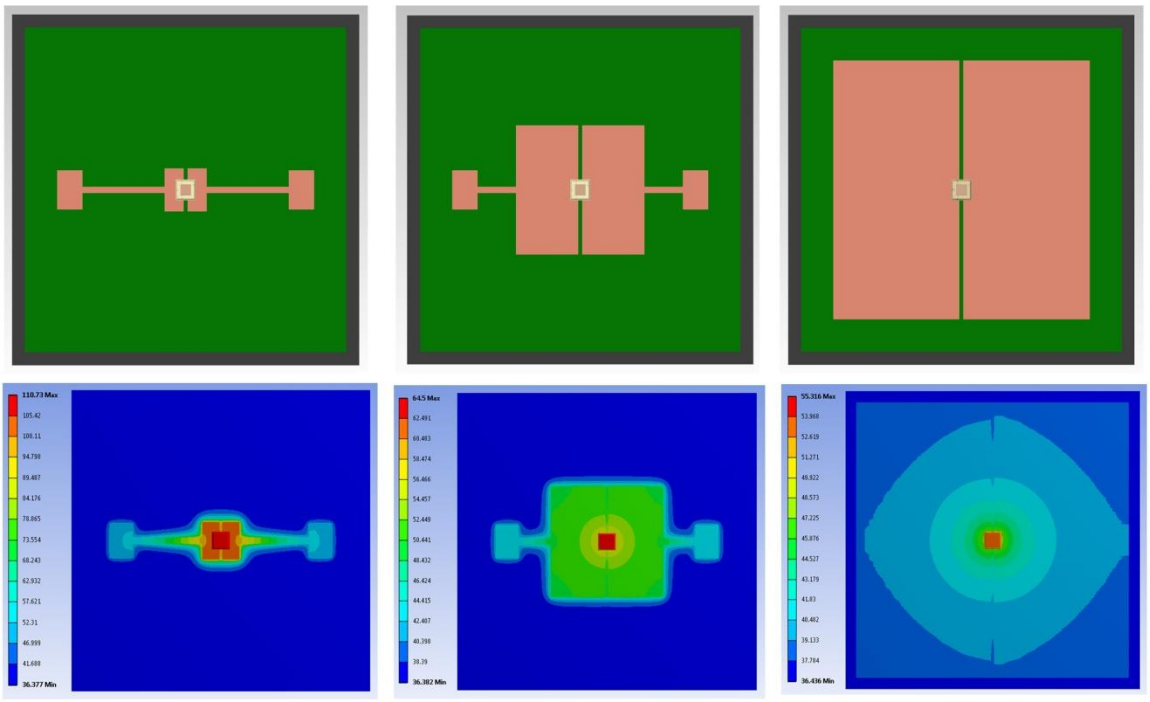

Fig. 43. Copper pad/trace schematics (top) and thermal simulations (bottom) for prototype LEDs driven at 1W on copper pad sizes of 3, 10, and 25mm (from left to right). The junction temperature of the LEDs (central small square) decreases significantly as pad size increases.

We investigated the effect of reducing copper trace area and thickness (and therefore cost), while understanding the trade-offs of such minimization with LED thermal management. Likewise, we considered the effect of changing the FR-PCB thickness on calculated LED junction temperature (T_j). We designed several copper trace pad sizes for individual prototype LEDs and both simulated and fabricated each combination of pad size, copper trace thickness, and FR-PCB thickness. Sample schematics and thermal simulation results for prototype LEDs driven at 1W electrical input power are shown in Fig. 43 for copper pad sizes of 3mm, 10mm, and 25mm.

Individual prototype LEDs were solder-attached to copper pads on FR4 to estimate LED junction temperature and thereby validate thermal simulations. As indicated in Fig. 44, for an example case of 70µm thick copper on two different thickness of FR-PCB there was very good agreement between simulations and measured results, with some minor deviation at the smallest pad size (which, as discussed below, was not likely be considered for this troffer design). This gave further confidence in the accuracy of the simulations in predicting LED junction temperature with various combinations of input power, copper trace/pad geometry, and circuit board characteristics.

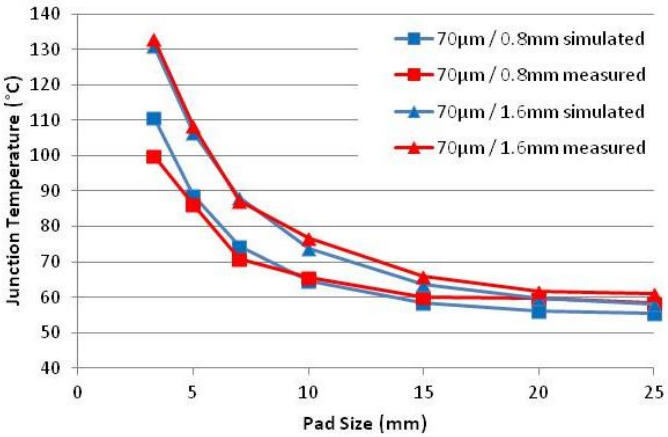

Fig. 44. Simulated (blue) vs. measured (red) LED junction temperature vs. pad size for 70µm thick copper on 0.8 and 1.6mm thick FR4. Simulated and measured data agree well with one another, validating the underlying models used in simulation.

The junction temperature of prototype LEDs was simulated for various copper square pad sizes (3.3mm to 25mm), three representative copper thicknesses (35, 70, 105µm), and two representative FR-PCB thicknesses (0.8, 1.6mm). In Fig. 45 the LED T_j is plotted as a function of pad size and copper thickness (left) and pad size and FR-PCB thickness (right) for an LED input power of 1W. In both cases, the calculated LED T_j was unacceptably high at the smallest copper pad sizes (*e.g.* 3.3mm, 5mm), but then quickly decreased to < 75°C for pad sizes of > 10mm. There was no appreciable difference between the 70µm and 105µm thick pads, which indicated copper thickness could be kept low to reduce cost. The effect of FR4 board thickness was also most pronounced at small copper pad size, with a 1.6mm thick board presenting higher thermal resistance to heat conduction (and therefore higher T_j values) than a 0.8mm board.

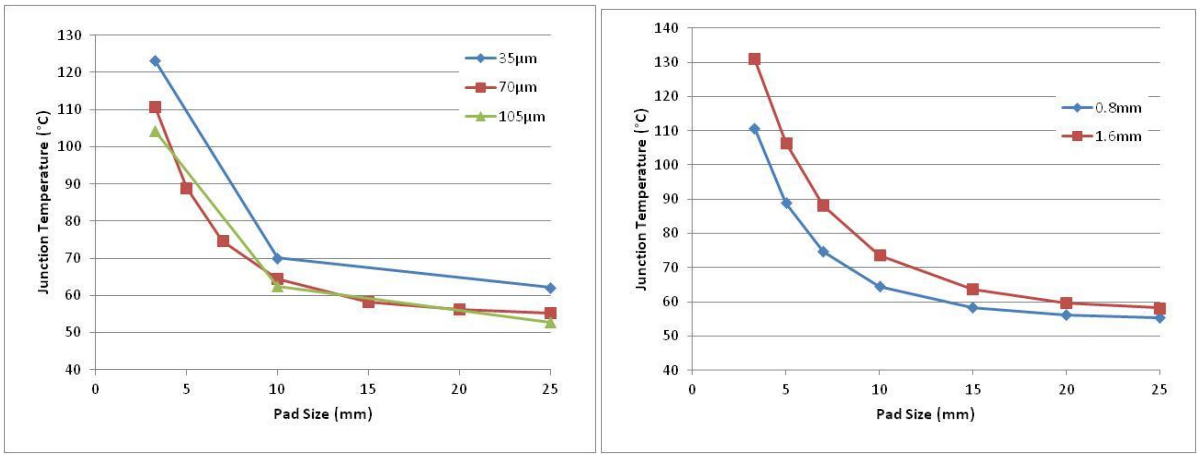

Fig. 45. Left: LED junction temperature vs. copper pad size for three copper thicknesses. Right: LED T_j vs. copper pad size for two FR-PCB thickness values. The LED junction temperature in both cases decreases rapidly as pad size increases, with a pad size of >10mm likely to result in a satisfactory LED T_j at this input power.

Thermal simulations predicted the feasibility of meeting our program requirement for low (< 6%) thermal roll-off by driving prototype packages at an optimal electrical input power level while spacing them appropriately (with the constraint that visible LED "pixelation" not be perceptible through the diffuser). Thermal modeling focused on simulating prototype packages on conventional fiberglass-reinforced epoxy laminate printed circuit board (FR-PCB), a low-cost baseline platform that can be readily measured for verification.

We placed arrays of prototype packages on FR-PCBs of 1.6mm thickness and 1" width, with representative copper trace thickness and coverage. Inter-LED spacing was set at 0.75", 2.25", and 3". The FR-PCBs were attached to steel sheet metal (such as typically used in troffer luminaires) with thermally conductive adhesive tape. To quantify thermal roll-off, the luminous flux of each LED array was measured in an "instant on" (short pulse) condition, and then during continuous (steady-state) operation until the luminous flux settled at a constant value (typically 15-20 min.). The LEDs were driven at current and voltage values that equated to an input power of 0.25W for each LED, and the whole array was tested inverted (LEDs facing down) in the integrating sphere to emulate normal operation of a ceiling-mounted troffer.

The results of this testing are summarized in Table 4, in which the luminous flux at steady state decreased by less than 3.1% for all conditions tested. Likewise, the solder point temperature remained at relatively low values (< 35°C), as predicted by earlier simulations for packages driven at 0.25W input power. These results indicated the promise of optimally distributed, low-power prototype LEDs in the troffer.

Table 4. Luminous flux values of prototype LED arrays soldered to FR-PCBs and mounted on sheet metal, in both "instant on" and "steady state" conditions at an input power of 0.25W per LED. The approximate solder-point temperature (T_{sp}) is included as well. All test conditions showed low (< 3.1%) thermal roll-off.

LED Spacing (inches)	**Instant-on LF** (lm)	**Stead-State LF** (lm)	**% LF drop**	**Approx. T_{sp}** (°C)
0.75	990.0	959.7	**3.1**	35
2.25	304.4	299.2	**1.7**	31
3.00	261.9	257.7	**1.6**	30

Task 4 – Luminaire Integration

The final direct-view demonstration troffer luminaire was assembled from: arrays of prototype LEDs fabricated to emit at the intended color temperature and CRI; low-cost printed circuit boards; a commercially available driver with current tuning capability; and a simplified mechanical housing adapted from Cree's AR24 troffer. The aim of this design was to minimize the number and complexity of manual assembly steps, and use as few fasteners and other "miscellaneous" small components as possible.

To create multiple populated PCBs, solder paste was applied to the boards using a large-area stencil mask (as is done in production); automated pick-and-place equipment was used to accurately locate LEDs on solder pads; and solder reflow was conducted to secure LEDs to the boards electrically and mechanically. After reflow, the boards were electrically tested to verify that all devices were in good electrical contact, which was the criterion for package attached yield. Among 540 LEDs that were attached to FR-PCBs, only two were found to have a bad connection to the board solder pads. This equated to a package attach yield of **99.7%**, exceeding our milestone target of 99.5%.

Rows of LED-populated FR-PCBs were attached directly to the troffer housing with thermally conductive tape, which was a conservative measure since LEDs on free-standing boards in air had been found to have only ~0.75% thermal roll-off (decrease in luminous flux after heating up) when driven at the intended steady-state forward current. In production, we

speculate that boards could be attached using cheaper tape or adhesives that are not thermally rated, since all heat dissipation occurs within the copper trace layer of the FR-PCBs. A broad-area diffuser was put in place, which consisted of a thin high-efficiency diffusion film mounted on an acrylic sheet for mechanical stability. The driver current was adjusted to the value determined in previous board-only DC testing, in order to reach the required luminous flux and efficacy.

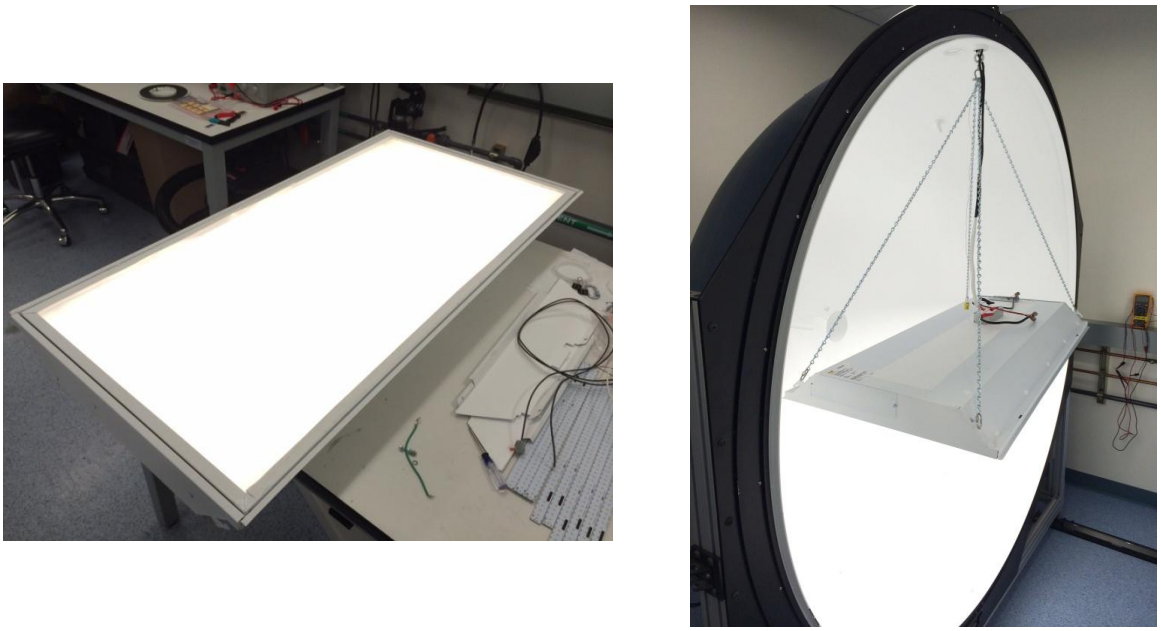

Fig. 46. Left: Demonstration troffer with diffuser in place. Right: Troffer mounted in integrating sphere for performance evaluation.

Troffer performance testing was conducted in a calibrated integrating sphere at SBTC (see Fig. 46 right). Luminous flux and efficacy were measured in "instant on" and "steady state" conditions, as well as with and without the diffuser and driver in place, in order to quantify optical, thermal, and driver efficiencies. The spectrum and color point of the troffer are shown in Fig. 47, which indicate that the troffer emits at a color point very near 3500K on the blackbody curve, as intended.

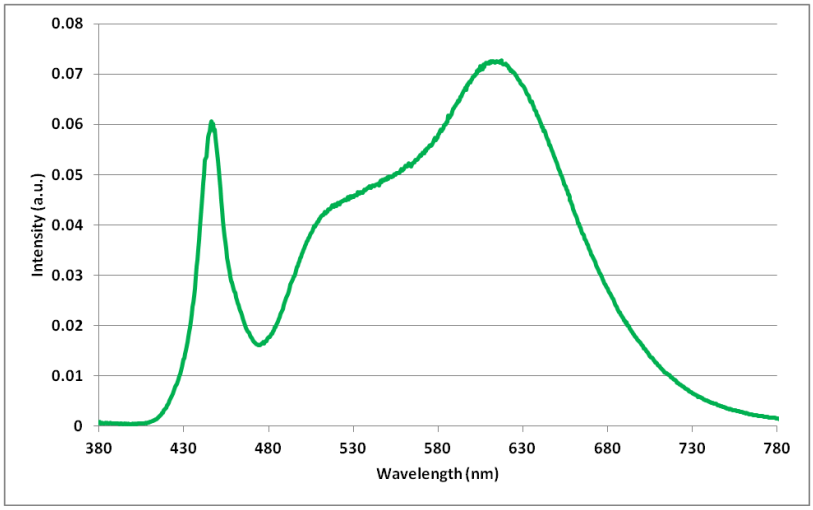

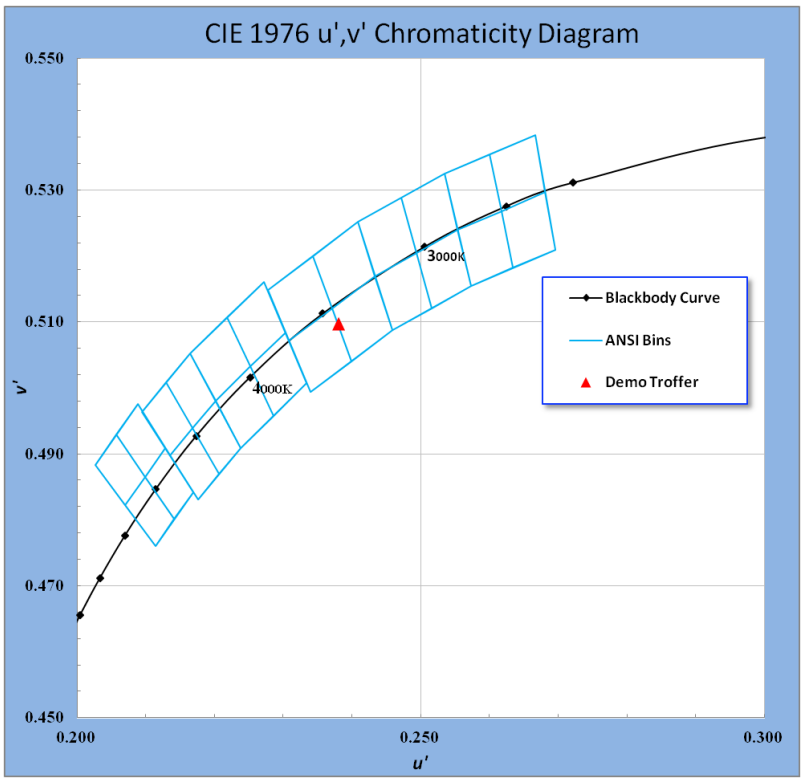

Fig. 47. Top: Spectrum of demonstration troffer. Bottom: Color point of troffer at steady state. The color point is very near 3500K on the blackbody curve.

The performance characteristics of the demonstration troffer are summarized in Table 5, showing that the troffer exhibited steady-state efficacy, luminous flux, and CRI values that were higher than targeted. Due to the relatively low input power per package, the thermal roll-off from instant-on to steady state was only **0.6%**, far less than the 6% that was targeted for the project. This enabled elimination of any heat sinks and use of low-cost FR-PCBs attached directly to the troffer housing. As mentioned above, this thermal efficiency also obviates the need for expensive thermally conductive adhesive or tape for mounting the PCBs to the housing.

Table 5. Measured characteristics of the fully assembled (including driver) demonstration troffer operating at steady state, as determined in a 2m calibrated integrating sphere.

Characteristic	**Value**	**Method**
Color Temperature	3385 K	Automated spectral calculation
Distance from blackbody locus (Duv)	-0.003	Automated spectral calculation
Color Rendering Index	93	Automated spectral calculation
Luminous Flux	4025 lm	Calibrated spectrometer
Luminous Efficacy	93.3 lm/W	Calibrated spectrometer, power meter
Wall-plug Efficiency	29.6%	Calibrated spectrometer, power meter
Optical Efficiency	90.9%	Comparison of luminous flux with and without diffuser in place
Thermal Efficiency	99.4%	Comparison of instant-on and steady-state luminous flux

We developed anticipated materials and assembly cost reduction figures for the demonstration troffer relative to the baseline CR24 troffer, which are illustrated in Fig. 48. Where necessary, component costs were scaled down to reflect typical discounts for production volumes. Via this new design, we exceeded the total cost reduction target of 30% by reducing costs in various subsystems. Light engine and mechanical/thermal subsystems costs were both lower by >30%. Driver and wiring costs were estimated to be reduced by ~35% due to the simpler circuitry needed for all-phosphor LEDs relative to the discrete TrueWhite® approach (blue+yellow and red-emitting packages) used in the CR24. In addition, anticipated assembly costs would be reduced by 35-40%, and a minor (~10%) reduction in packaging/overhead/freight costs was assumed due to the lower-weight design presented by the simplified direct-view housing. In total, a manufacturing cost reduction of over 31% was estimated. We met the cost-reduction milestone for the light engine, and nearly met the milestone for the mechanical subsystem cost reduction.

Fig. 48. Cost reductions enabled by the demonstration luminaire architecture relative to Cree's CR24 luminaire at program start. Pie chart areas are scaled by total cost.

Milestones / Deliverables

Year 1

Title: **Custom primary optic configuration defined.**
Success Criteria: Down-selection of primary lens size, shape and material.
Planned Date: 4/1/13
Verification Method: Details of the data based decision for down selection were documented in a report.
Progress: This milestone was completed on time. The exterior geometry (including package lens, *i.e.* primary optic) of the new prototype package was established, as was its constituent materials and a reproducible method for its fabrication.

Title: **White LED component with custom primary optic providing 95% optical efficiency compared to the conventional hemispherical lens LED.**
Success Criteria: Complete the design, fabrication and testing of the LED package with its custom primary optic.
Planned Date: 8/1/13
Verification Method: Integrating sphere measurements in a controlled ambient condition environment will be used to compare conventional components to the new prototype component. The results will be documented in a report.
Progress: This milestone was completed ahead of schedule. We established that the efficacy of the prototype LED package was comparable to that of similarly sized conventional Cree packages with a hemispherical domed lens, when driven at the same input power.

Title: **Light engine with COB platform providing 97% process yield.**
Success Criteria: Achieving at least 97/100 successful attach procedures when using the established process methodology.
Planned Date: 8/1/13
Verification Method: Thermal resistance measured with thermocouples and infrared imaging coupled with shear strength testing will be used to quantify attach capability.
Progress: This milestone was completed on time, with an automated pick and place prototype LED component attach yield of 99%, based on forward voltage and luminous flux measurements.

Title: **Specification for fixture design with integrated thermal management completed.**
Success Criteria: Design submitted to prototype metal shop for fabrication.
Planned Date: 8/1/13
Verification Method: Thermal modeling will be used to guide prototype designs which will subsequently be tested with various heat loads for performance validation.
Progress: Completed on time for thermal simulation cases involving prototype LED packages on PCBs with copper traces. We conducted similar simulation and testing protocols on alternate materials and geometries.

Title: **Diffusing optics design requirement specified based on selected primary lens design from Task 2.**
Success Criteria: Design submitted to prototype metal shop for fabrication.
Planned Date: 8/1/13
Verification Method: Using measured light engine optical performance data (intensity and color distributions), perform optical modeling to design the most efficient optic that meets the requirements of color mixing.
Progress: This milestone was completed on time based on system optical performance data gathered for various diffuser types and geometries. We used these data as design guidelines during later months of the program when the full-scale demonstration luminaire was being constructed.

Year 2

Title: **LED primary optic manufacturing process selected**.
Success Criteria: Down select from various options and procure necessary tooling and materials.
Planned Date: **11/1/13**
Verification Method: Integrating sphere and goniophotometer data will be used to quantify primary optic performance.
Status: Completed on schedule. Progress in developing a highly reflective coating for the prototype LED substrate surface confirmed that it could be reproducibly applied using high-volume techniques, without the need for modification of existing automated phosphor application, chip placement, or primary optic (lens) molding methods.

Title: **LED with custom primary lens showing >90% lumen maintenance after 500 hours accelerated testing and color point shift (u' and v') within a 5-step MacAdam ellipse.**
Success Criteria: Measure > 90% lumen maintenance and color point shift (u' and v') within a 5-step MacAdam ellipse after 500 hours of reliability testing.
Planned Date: **11/1/13**
Verification Method: LED samples will be fabricated and output verified using a calibrated integrating sphere measurement system at intervals of 168 hours until 504 hours reliability testing has been completed.
Status: Completed ahead of schedule, with more than 840 hrs. accelerated testing completed on prototype packages with a reflective substrate coating.

Title: **Fixture thermal roll-off (instant-on to steady state) at 10%.**
Success Criteria: Measure >90% luminous flux after reaching a steady state temperature.
Planned Date: **11/1/13**
Verification Method: Samples will be fabricated and output verified using a calibrated integrating sphere measurement system at initial turn on and at later time intervals until thermal equilibrium has been obtained as measured with thermo couples attached to different locations on the luminaire.
Status: Completed on time, with prototype LED package arrays on PCBs mounted to sheet metal.

Title: **Light Diffusing optics lens fabricated with ≥ 85% optical efficiency.**
Success Criteria: Measure >85% optical efficiency with a diffusing optic in place.

Planned Date: **11/1/13**
Verification Method: Samples will be fabricated and output verified using a calibrated integrating sphere measurement system with and without the diffusing optic in place.
Status: Completed early, with several diffuser types exhibiting >93% optical efficiency when tested on representative luminaire test beds.

Title: **LED board integration process selected.**
Success Criteria: Down selection of process choices.
Planned Date: **2/1/14**
Verification Method: Details of the data based decision for down selection will be documented in a report.
Status: Completed on time. A combination of thermal modeling and experimental measurements in an integrating sphere verified that the thermal characteristics of prototype LED arrays on PCBs was well within an acceptable range.

Title: **Fixture surface luminance of 20 lumens/in^2.**
Success Criteria: Measure luminance of 20 lumens/in^2.
Planned Date: **2/1/14**
Verification Method: Samples will be fabricated and the luminance will be verified using a calibrated luminance meter.
Status: Completed on time. The average luminous flux per unit area was routinely measured to be larger than the target of 20 lm/in^2 using representative LED drive currents, LED-LED spacings, and LED-diffuser spacings.

Title: **LED light engine providing with 5200 lumens at 3500K CCT and CRI of 90.**
Success Criteria: Measure > 5200 lumens at 3500K CCT and CRI of 90.
Planned Date: **5/1/14**
Verification Method: Samples will be fabricated and output verified using a calibrated integrating sphere measurement system.
Status: Completed on time, with a prototype light engine emitting ~5300 lm at steady state.

Title: **Diffusing optics lens fabricated with ≥ 90% optical efficiency.**
Success Criteria: Measure >90% optical efficiency with a diffusing optic in place.
Planned Date: **5/1/14**
Verification Method: Samples will be fabricated and output verified using a calibrated integrating sphere measurement system with and without the diffusing optic in place.
Status: Completed early, with several diffuser types exhibiting >93% optical efficiency when tested on representative luminaire test beds.

Title: **Fixture thermal roll-off (instant-on to steady state) at 6%.**
Success Criteria: Measure >94% luminous flux after reaching a steady state temperature.
Planned Date: **5/1/14**
Verification Method: Samples will be fabricated and output verified using a calibrated integrating sphere measurement system at initial turn on and at later time intervals until thermal equilibrium has been obtained as measured with thermo couples attached to different locations on the luminaire.

Status: Completed on time, with a prototype light engine having a thermal roll-off of 4.4%.

Title: **Light engine with COB platform providing 99.5% process yield.**
Success Criteria: Achieving at least 199/200 successful attach procedures when using the established process methodology.
Planned Date: **8/1/14**
Verification Method: Thermal resistance measured with thermo couples and infrared imaging coupled with shear strength testing will be used to quantify attach capability.
Status: Completed on time. A solder attach yield of 99.7% was reached.

Title: **LED with custom primary lens showing >90% lumen maintenance after 1000 hours accelerated testing and color point shift (u' and v') within a 4-step MacAdam ellipse.**
Success Criteria: Measure > 90% lumen maintenance and color point shift (u' and v') within a 4-step MacAdam ellipse after 1000 hours of reliability testing.
Planned Date: **8/1/14**
Verification Method: Samples will be fabricated and output verified using a calibrated integrating sphere measurement system at intervals of 168 hours until 1008 hours reliability testing has been completed.
Progress: Completed on time, with prototype packages passing several thousand hours of accelerated lifetime testing.

Title: **LED light engine cost reduced 23% over the light engine cost for the CR24 troffer product.**
Success Criteria: Calculate cost versus present technology to verify cost is reduced by 23%.
Planned Date: **8/1/14**
Verification Method: Calculate bill of materials, and labor depreciation and over head for the new product and compare it to current values for product sold in the market place.
Status: Completed on time. An estimated reduction of ~30% was achieved.

Title: **Prototype mechanical fixture with a cost reduction of 33% over the mechanicals cost for the CR24 troffer product.**
Success Criteria: Calculate cost versus present technology to verify cost is reduced by 33%.
Planned Date: **8/1/14**
Verification Method: Calculate bill of materials, and labor depreciation and over head for the new product using factory models and compare it to current known values for product sold in the market place.
Status: This milestone was nearly met, with an estimated mechanical subsystem cost reduction of ~31%.

PRODUCTS

A chief project accomplishment was the successful development of a new compact, high-efficacy LED component geometry with a broad far-field intensity distribution and even color point vs. emission angle. After further optimization and testing for production, the Cree XQ series of LEDs resulted. XQ LEDs are currently utilized in Cree's AR series troffers, and they are being considered for use in other platforms. The XQ lens geometry influenced the later

independent development of Cree's XB-E and XB-G high-voltage LEDs, which also have a broad intensity distribution at high efficacy and are finding wide implementation in Cree's omnidirectional A-lamps.